

Article

# Sedimentology and Diagenesis of the Early–Middle Eocene Carbonate Deposits of the Ceno-Tethys Ocean

Ahmer Bilal <sup>1</sup> , Renchao Yang <sup>1,2,\*</sup>, Muhammad Saleem Mughal <sup>3</sup>, Hammad Tariq Janjuhah <sup>4,\*</sup> ,  
Muhammad Zaheer <sup>3</sup> and George Kontakiotis <sup>5</sup> 

- <sup>1</sup> Shandong Provincial Key Laboratory of Depositional Mineralization & Sedimentary Minerals, Shandong University of Science and Technology, Qingdao 266590, China  
<sup>2</sup> Laboratory for Marine Mineral Resources, Qingdao National Laboratory for Marine Science and Technology, Qingdao 266071, China  
<sup>3</sup> Institute of Geology, University of Azad Jammu and Kashmir, Muzaffarabad 13100, Pakistan  
<sup>4</sup> Department of Geology, Shaheed Benazir Bhutto University, Sheringal 18050, Pakistan  
<sup>5</sup> Department of Historical Geology-Paleontology, Faculty of Geology and Geoenvironment, School of Earth Sciences, National and Kapodistrian University of Athens, Panepistimiopolis, Zografou, 15784 Athens, Greece  
\* Correspondence: r.yang@sdust.edu.cn (R.Y.); hammad@sbbu.edu.pk (H.T.J.)

**Abstract:** An integrated study based on field observation, petrography, and scanning electron microscopy (SEM) on the Early–Middle Eocene carbonate rocks has been carried out, which were deposited in the Ceno-Tethys Ocean. The study area of the Yadgaar Section lies on the eastern margin of the Upper Indus Basin, Pakistan. The Early–Middle Eocene Margalla Hill Limestone and Chorgali Formation act as reservoir rocks in other parts of the basin and are also present in the Yadgaar Section. The lack of comprehensive study in this area makes these reservoir rocks highly attractive for sedimentological evaluations and future exploration of hydrocarbons. The Early–Middle Eocene carbonate rocks are divided into nine microfacies: dolomitic foraminiferal mudstone–wackestone microfacies (EMI); green algae dominated, mixed foraminiferal wackestone–packstone microfacies (EMII); ostracod, green algae and gypsum dominating mudstone–wackestone microfacies (EMIII); algae and mixed foraminiferal wackestone–packstone microfacies (EMIV); *Nummulites* dominating mudstone–wackestone microfacies (EMV); algal limestone mudstone microfacies (EMVI); *Assilina* bed wackestone–packstone microfacies (EMVII); micritized larger benthic foraminiferal wackestone–packstone microfacies (EMVIII); and algal limestone, mudstone microfacies (EMIX). The transgressive–regressive environment in the Ceno-Tethys Ocean leads to the deposition of these microfacies in the platform interior, open marine platform, platform edge, platform margin reef, toe of the slope apron, arid–humid platform interior, platform edge, open marine platform interior, and restricted marine platform interior, respectively. Initial post-depositional diagenetic stages are identified from the base to the top of the strata by their respective cement types, i.e., the base–lower middle part of the strata demonstrates an eogenetic sub-stage with the appearance of drusy cement, the middle section indicates a mesogenetic sub-stage by the appearance of blocky cement, while the top portion again reveals an eogenetic sub-stage of diagenesis by the presence of drusy and blocky types of cement. The ascending–descending hierarchy of cement generations is directly proportional to the grade of diagenesis from the base to the top of the carbonate strata. Variable diagenetic effects on the various microfacies also increase the secondary porosity range and enhance the reservoir characteristics of the Formations. The presence of foraminifera microfossils determined that these carbonate formations date from the Early–Middle Eocene.

**Keywords:** cement generation; diagenesis; gypsum; hydrocarbons; microfacies; source rock



**Citation:** Bilal, A.; Yang, R.; Mughal, M.S.; Janjuhah, H.T.; Zaheer, M.; Kontakiotis, G. Sedimentology and Diagenesis of the Early–Middle Eocene Carbonate Deposits of the Ceno-Tethys Ocean. *J. Mar. Sci. Eng.* **2022**, *10*, 1794. <https://doi.org/10.3390/jmse10111794>

Academic Editor: János Kovács

Received: 18 October 2022

Accepted: 17 November 2022

Published: 21 November 2022

**Publisher's Note:** MDPI stays neutral with regard to jurisdictional claims in published maps and institutional affiliations.



**Copyright:** © 2022 by the authors. Licensee MDPI, Basel, Switzerland. This article is an open access article distributed under the terms and conditions of the Creative Commons Attribution (CC BY) license (<https://creativecommons.org/licenses/by/4.0/>).

## 1. Introduction

In the Eocene age, carbonate strata were deposited on the shallow carbonate platform due to the complex lagoonal conditions of the Ceno-Tethys Ocean. Green and coralline

algae, along with benthic foraminifera from Tethyan deposits, are worldwide proven to be excellent indicators of paleoenvironmental settings [1]. A high abundance of benthic foraminiferas in shallow marine Tethyan rocks indicates high temperature after the Paleocene Eocene thermal maximum (PETM) or middle Eocene Climatic Optimum [2,3]. *Assilina* beds and *Alveolina*-rich microfacies in early Lutetian are an indicator of a hyperthermal event in shallow marine platform deposits of this time of the Tethys Ocean [1,4]. Micritic carbonate strata represent these deposits with shallow shelf carbonate ramp and inner platform settings in the Tethys Ocean [5].

The rocks of the Upper Indus Basin's (UIB) geology range in age from Precambrian to recent [6,7]. However, in the Yadgaar Section, only the Cambrian to Miocene rock sequence is exposed [8]. Sandstone and carbonate strata of Paleocene–Eocene rocks are unconformably overlain by Cambrian-aged dolomite of the Abbottabad Formation. The sandstone sequence is represented by the early Paleocene Hangu Formation, while the late Paleocene carbonate rocks are represented by the Lockhart Limestone and Patala Formation [9]. The Patala Formation and Lockhart Limestone's upper and lower contacts, respectively, are marked as unconformable. Many researchers worked on Eocene Tethyan deposits regionally [1–3,10–12]. The Early–Middle Eocene nodular to fused nodular carbonate deposits of Pakistan are represented by the Margalla Hill Limestone and the Chorgali Formation, respectively. The Kohat, Potwar, Abbottabad, and Murree regions are further UIB locations where these deposits were observed. This comprehensive petrological investigation demonstrates a variance in microfauna and depositional settings between those zones and the targeted area, despite the limited aspects of research in those areas [13–17]. These rocks are present in the study area of the Yadgaar section of the UIB. However, only a few researchers in the UIB and surrounding areas have focused on these rocks and their coeval strata. These previous researchers targeted only individual Formations and their limited aspects [13–16,18–21]. These deposits are unconformably underlain by sandstone rocks of the Eocene–Oligocene-aged Kuldana Formation. The Kuldana Formation is finally overlain unconformably by the Murree Formation in the study area [8,17].

A comprehensive petrological, paleontological, and sedimentological study of Early–Middle Eocene rocks in the Yadgaar Section of the UIB is still missing to unfold microfacies variations, depositional settings, and post-depositional diagenetic stages and their effect on their reservoir characteristics for possible hydrocarbon exploration in the future (Figure 1). The goal of the current study is to carry out a combined and comprehensive evaluation of Early–Middle Eocene rocks to determine their age, depositional environment, diagenetic stages and tectonic settings of the area during and after the deposition of these rocks by detailed petrographical, sedimentological, paleontological, and mineralogical investigations.

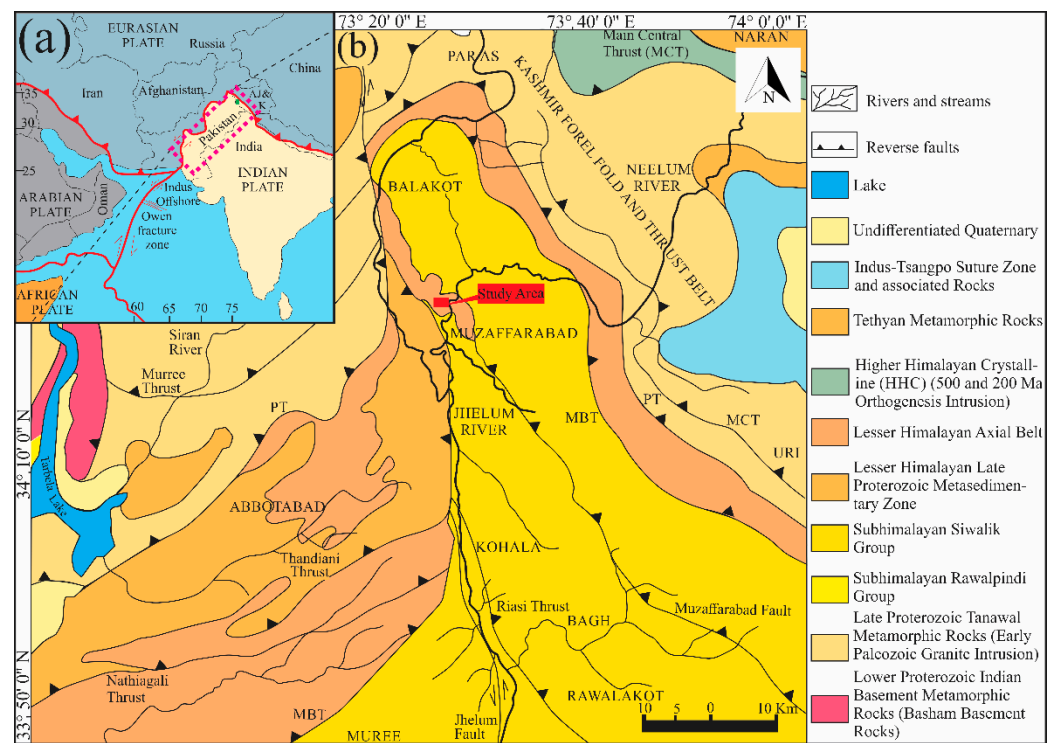


**Figure 1.** (a) Inset shows the regional location of Indus Basin in Pakistan with the dotted purple line; (b) study area of the Yadgaar Section in the UIB.

**2. Material and Methods**

*2.1. Fieldwork*

Fieldwork involved identification of Early–Middle Eocene Margalla Hill Limestone and the Chorgali Formation’s upper and lower contacts and recognition of outcrop lithofacies (Figure 1). For the petrographic evaluation, 44 representative fresh rock samples were collected from the outcrop of Margalla Hill Limestone (Table 1) and 32 samples from the Chorgali Formation (Table 2). The Jacob’s Staff technique was used to measure the thickness of the section, which was used to help determine the lithology of the section. In the lab of the Institute of Geology at the University of Azad Jammu and Kashmir, thin sections were prepared.

**Table 1.** Modal mineralogical composition of the Early–Middle Eocene carbonate rocks of Yadgaar Section. (CM-carbonaceous material).

S. No.	Spar (%)	Micrite (%)	Bioclasts (%)	CM (%)	Pyrite (%)	Henatite (%)	Gypsum (%)	Dolomite (%)	Calcite Vein (%)	Dunham Classification
YMG1	2	10	10	2	4	7	-	65	-	Mudstone–Wackestone
YMG2	1	13	8	2	4	5	-	67	-	
YMG3	3	10	11	3	2	6	-	65	-	
YMG4	2	9	12	2	6	6	-	63	-	
YMG5	7	28	40	2	2	7	1	5	8	
YMG6	5	31	40	2	2	7	1	4	8	
YMG7	7	33	38	3	2	5	1	4	7	
YMG8	6	26	42	2	3	5	1	5	10	

Table 1. Cont.

S. No.	Spar (%)	Micrite (%)	Bioclasts (%)	CM (%)	Pyrite (%)	Hematite (%)	Gypsum (%)	Dolomite (%)	Calcite Vein (%)	Dunham Classification
YMG9	7	32	50	1	4	1	1	4	-	Wacke-packstone
YMG10	7	35	48	1	3	1	1	4	-	
YMG11	5	32	51	1	3	2	1	5	-	
YMG12	7	30	52	1	2	1	1	6	-	
YMG13	14	10	53	1	1	2	1	15	2	
YMG14	18	10	54	1	1	2	1	10	3	
YMG15	21	8	55	1	1	1	1	9	3	
YMG16	18	9	53	2	2	2	2	10	2	
YMG17	5	26	50	2	2	5	2	5	3	
YMG18	5	24	52	2	3	5	2	3	4	
YMG19	5	29	47	1	2	6	2	5	3	
YMG20	4	35	45	1	4	3	3	3	2	
YMG21	3	62	15	2	3	6	1	7	1	
YMG22	2	66	14	2	2	5	2	6	1	
YMG23	4	58	14	3	3	7	2	8	1	
YMG24	4	59	16	2	1	7	1	9	1	
YMG25	5	56	10	2	1	8	2	15	-	
YMG26	6	55	10	2	1	8	2	16	-	
YMG27	3	52	12	3	1	9	2	18	-	
YMG28	5	50	14	3	1	10	2	15	-	
YMG29	3	57	30	2	1	6	-	-	1	
YMG30	5	57	28	3	1	5	-	-	1	
YMG31	2	56	33	2	1	5	-	-	1	
YMG32	3	57	30	4	1	4	-	-	1	
YMG33	10	22	60	2	2	4	2	2	1	
YMG34	10	24	51	2	1	6	1	2	1	
YMG35	7	20	58	2	2	5	1	2	1	
YMG36	8	22	56	1	3	5	1	3	1	
YMG37	5	30	50	2	4	6	-	3	1	
YMG38	5	30	51	2	4	4	-	3	1	
YMG39	3	32	49	3	5	4	-	3	1	
YMG40	4	28	50	2	6	5	-	4	1	
YMG41	-	60	12	2	4	5	1	15	1	
YMG42	-	62	12	1	4	6	1	13	1	
YMG43	-	64	10	1	3	3	1	16	1	
YMG44	-	64	10	4	3	2	1	15	1	

Table 2. Modal mineralogical composition of the Early–Middle Eocene carbonate rocks of Yadgaar Section.

	Spar (%)	Micrite (%)	Bioclasts (%)	CM (%)	Pyrite (%)	Hematite (%)	Chert/Chalcedony (%)	Gypsum (%)	Dolomite (%)	Calcite Vein (%)	Dunham Classification
YCF1	-	20	2	20	2	8	1	2	37	8	Mudstone
YCF2	-	22	2	20	1	6	1	2	38	8	
YCF3	-	21	3	18	2	7	1	2	39	7	
YCF4	-	20	4	20	1	8	1	2	39	5	

Table 2. Cont.

	Spar (%)	Micrite (%)	Bioclasts (%)	CM (%)	Pyrite (%)	Hematite (%)	Chert/ Chalcedony (%)	Gypsum (%)	Dolomite (%)	Calcite Vein (%)	Dunham Classification
YCF5	3	5	50	20	1	3	1	2	15	-	Wacke-packstone
YCF6	3	5	59	15	1	3	1	2	11	-	
YCF7	4	8	48	17	1	3	1	3	15	-	
YCF8	3	9	55	13	1	3	1	2	14	-	
YCF9	4	5	54	15	3	3	-	2	14	-	
YCF10	4	7	53	16	3	2	-	2	13	-	
YCF11	6	9	48	13	4	3	-	3	14	-	
YCF12	4	8	56	11	3	2	-	2	14	-	
YCF13	10	7	39	10	2	-	2	2	25	3	
YCF14	10	10	40	12	2	-	1	2	20	3	
YCF15	9	10	39	10	3	-	1	2	23	3	
YCF16	14	8	33	14	1	-	1	3	22	4	
YCF17	10	6	44	12	2	-	-	3	20	3	Wackestone
YCF18	13	17	29	16	1	-	-	3	18	3	
YCF19	12	13	28	19	1	-	-	2	23	2	
YCF20	12	15	30	18	-	-	-	2	20	3	
YCF21	5	32	25	13	3	2	1	7	10	2	
YCF22	3	31	28	12	3	2	1	6	12	2	
YCF23	1	38	23	13	2	1	1	7	10	4	
YCF24	-	39	25	13	2	1	1	7	9	3	
YCF25	-	20	4	23	-	-	2	1	40	10	
YCF26	-	18	5	27	-	-	1	1	38	10	
YCF27	-	17	4	28	-	-	2	1	36	12	Mudstone
YCF28	-	19	4	27	-	-	2	1	37	10	
YCF29	-	39	2	16	2	1	5	1	4	30	
YCF30	-	66	1	11	2	-	6	1	2	11	
YCF31	-	66	2	9	2	1	5	1	3	11	
YCF32	-	64	1	11	2	-	5	1	3	13	

## 2.2. Petrography

A petrographic study of limestone samples collected from the Early–Middle Eocene rocks of the Yadgaar Section (Figure 2; Table 1) was carried out in the mineralogy/ petrology laboratory of the University of Azad Jammu and Kashmir. A LEICA-DM 750P polarized microscope and a LEICA-S6D stereo zoom microscope were used to find out the modal mineralogy, bioclast identification, and microfacies division from these thin sections. A LEICA-EC3 camera was used to acquire photomicrographs of fossils and other microscopic features.

## 2.3. Scanning Electron Microscopy (SEM)

Limestone and shale samples were studied under a scanning electron microscope (SEM) manufactured by JEOL Japan at the Hi-Tech Laboratory of the University of Azad Jammu and Kashmir. Rock samples were placed on a stud for sputter coating with platinum. The JFC-1600 auto fine coater (JEOL, Japan) was used to make the coating, which makes the image results of the non-conducting material the clearest to study. SEM analysis was carried out to examine the cement types and generations, which was further used to interpret the grade of diagenesis. This helped us figure out more about how the Margalla Hill Limestone and Chorgali Formation in the study area could be used as a reservoir.

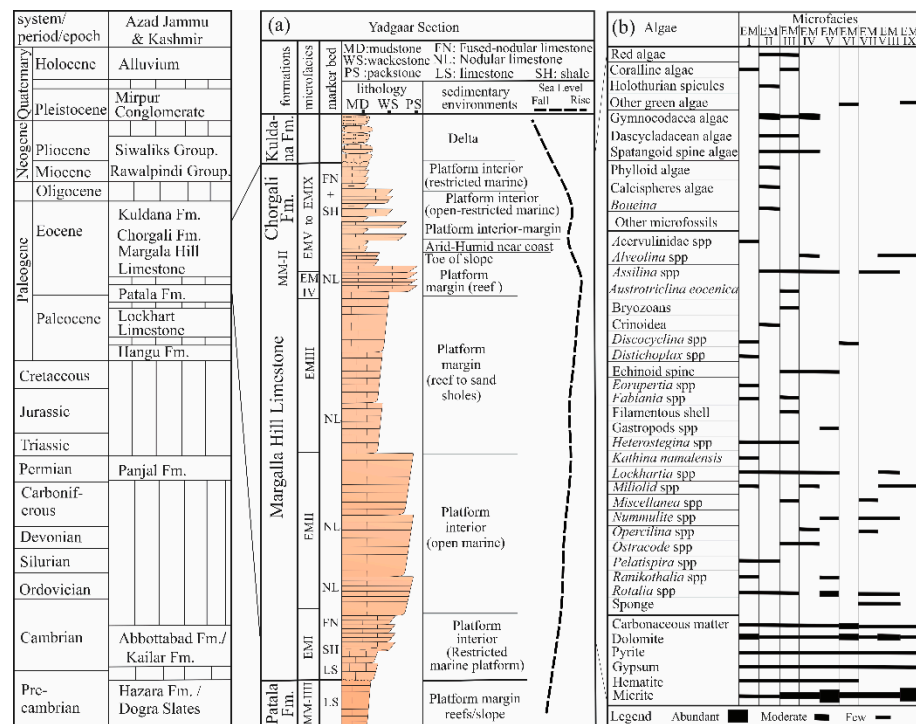


**Figure 2.** (a) Litholog of the Early–Middle Eocene carbonate rocks from the Yadgaar Section; (b) microfossils identified from the studied section. MD, Mudstone; FN, Fused nodular limestone; WS, Wackestone; NL, Nodular limestone; PS, Packstone; LS, Limestone; SH, Shales.

### 3. Results and Discussion

A shallow carbonate shelf existed in the Ceno-Tethys Ocean’s margins during the Early–Middle Eocene. This led to the deposition of micritic and well-developed nodular to fused nodular limestone rocks in the area (Figures 2 and 3). The resultant Margalla Hill Limestone and the Chorgali Formation were economically highly important as they are proven reservoirs in the other areas of the UIB.

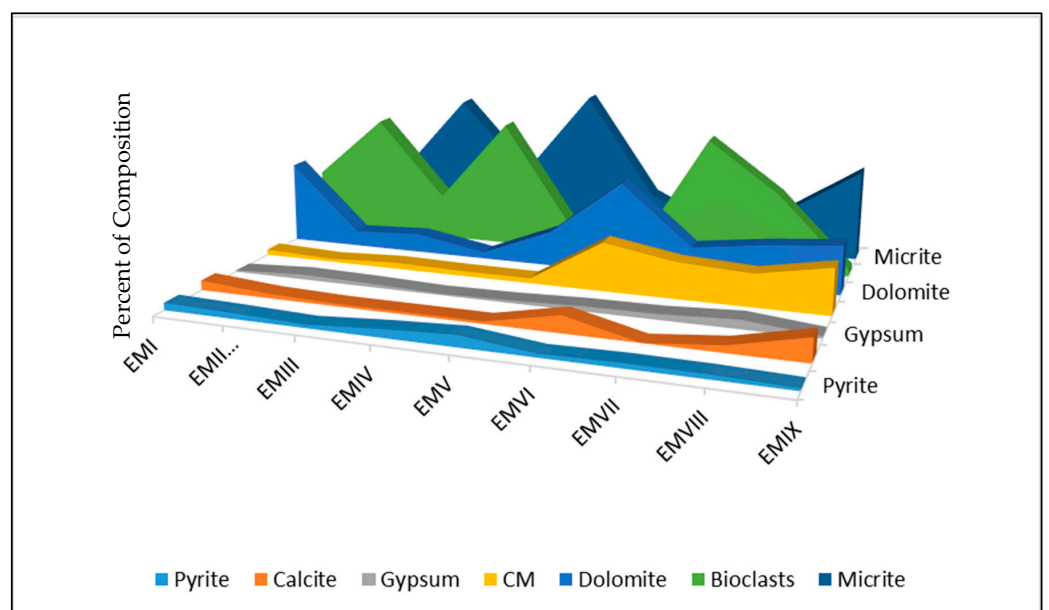


**Figure 3.** Graphic representation of Table 1. CM, carbonaceous material.

### 3.1. Lithofacies of the Early–Middle Eocene Carbonate Rocks

In the Yadgaar Section of the UIB, Early–Middle Eocene carbonate sequences have been divided into two stratigraphic units, i.e., the Margalla Hill Limestone and the Chorgali Formation. These Formations are dominantly comprised of nodular limestone in the lower part and limestone with shale intercalations in the upper part. Limestone interbedded with shale in the upper part ranges from 0.07 to 0.3 m in thickness (Figure 2). Dark brown–black colored shale exhibits carbonaceous material in its upper part. Based on the lithological variations in the field, nine lithofacies were identified.

An erosional unconformable lower contact of the Margalla Hill Limestone has been marked with the underlying Patala Formation. The first lithofacies is comprised of a 3-m-thick limestone bed and a 2-m-thick limestone bed that has intercalation of shale (Figure 4a). Light grey–bluish colored limestone is strongly compacted and hard. Shales were observed with limestone beds, and they are thin, ranging from 0.01 to 0.03 m. This lithofacies is 5 m in thickness. The second nodular limestone lithofacies is comprised of four beds of equally thick nodular limestone (Figure 4b). Each bed is 1.5 m in thickness; however, the fourth bed is a little deformed in the type section. Color variation is not marked and is found to be similar to the first lithofacies. The total thickness of this lithofacies is 4.5 m. The third marine nodular limestone lithofacies is light blue–dark dull colored and thick-bedded. The size of the nodules gradually increases from 0.07 to 0.15 m. Calcite veins (Figure 4c) are frequently observed in the outcrops. A high amount of carbonaceous material is clearly observed and distinguished in outcrops by a dull black color (Figure 4d). The thickness of this lithofacies is 30 m in the Yadgaar Section.

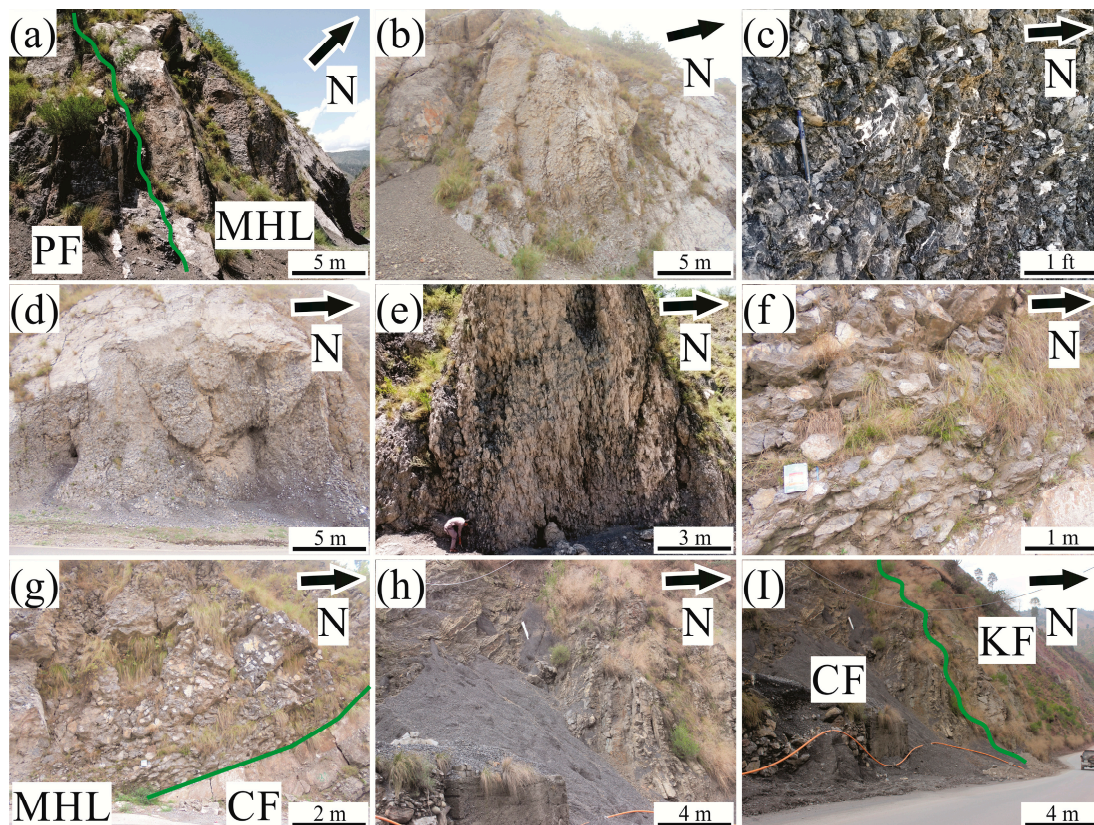


**Figure 4.** Photomicrographs showing (a) lower erosional unconformable contact of Patala Formation (PF) and Margalla Hill Limestone (MHL); (b) second nodular lithofacies; (c) calcite veins in third lithofacies; (d) carbonaceous material in third lithofacies; (e) massive nodular lithofacies; (f) nodular limestone; (g) contact between fifth and sixth lithofacies; (h) limestone and shale alteration lithofacies; and (I) upper erosional contact between Chorgali Formation (CF) and Kuldana Formation (KF).

The fourth lithofacies is a light brown color, nodular, and thick-bedded. The distinguishing feature of this microfacies is the decrease in carbonaceous content and the appearance of a light brown rusty colored limestone. Nodule sizes have also started to decrease in outcrops. The thickness of this lithofacies is also 30 m. The fifth lithofacies is a dark–light bluish grey colored, thick-bedded nodular lithofacies (Figure 4e). The rusting color starts to decrease, while the light–dark blue color starts to increase towards the top of the lithofacies. Carbonaceous content also starts to increase in this lithofacies. The distinguishing feature of this microfacies is the increasing concentration and maximum size of the nodules. The individual nodule size is  $0.12 \times 0.20$  m in width and height, respectively. This lithofacies is 20 m in thickness. The sixth lithofacies is also nodular on top but medium–small bedded (Figure 4f,g). Carbonaceous content is found to decrease and the thickness of this lithofacies is 20 m. The upper contact is marked planar with the Chorgali Formation in the study area.

The seventh lithofacies is dark grey in color and medium bedded in the study area. Fossils were not found in any outcrops of this lithofacies. In the study area, thin shales are found interbedded with limestone. This lithofacies is 5 m inches in thickness. The eighth lithofacies is a dark grey colored limestone with interbedded shale (Figure 4h). This lithofacies is highly fossiliferous and fossils are exposed on surfaces and observable with a hand lens. This lithofacies is 15 m in thickness. Above this, there is another difference between these middle Eocene rocks and the deltaic limestone facies of the late Eocene–Oligocene Kuldana Formation (Figure 4I).

### 3.2. Microfacies Characterization

Early–Middle Eocene rocks are comprised of nodular limestone beds and shales in the Yadgaar section. A gradual transition from light bluish grey to dark grey is observed while moving from the base towards the top. Limestone beds are nodular and medium–thick bedded from base to center, while medium–thin bedded and fused nodules are found in the upper most part of the section. Large benthic foraminifers are frequently observed throughout the samples. Shales can be observed in a minor amount at the base; however, a considerable amount of shale with interbedded limestone is present in its upper most part. As compared to the light grey shale at the base, the color of the shale is much darker at the top due to the presence of carbonaceous material.

A petrographic study of the Early–Middle Eocene carbonate rocks revealed that micrite and bioclasts are the dominant constituents. However, dolomite, carbonaceous material, pyrite, spar, and hematite are unequally distributed throughout the Formation. Gypsum is also found throughout the section in an almost equal but minor amount. Furthermore, chert is noted only in the upper stratigraphic unit (Chorgali Formation) in minor amounts. Dunham's classification is used to categorize the limestone samples studied under thin sections. This reveals different rock types of Early–Middle Eocene carbonate strata from base to top as: mudstone–wackestone, wackestone–packstone, packstone–wackestone, mudstone–wackestone, mudstone, wackestone–packstone, wackestone, and mudstone, respectively. Detailed petrographic studies indicate different grain sizes, textural compositions, and fossil types. The average grain size in the Formation is 0.02 mm, while the bioclast sizes range from 0.1 to 30 mm in length in these strata.

Different types of rocks are categorized on the basis of the Dunham [22] classification scheme. Nine different microfacies were categorized on the basis of biofacies (differences in fossil types) and these different rock types: (1) dolomitic foraminiferal mudstone–wackestone microfacies (EMI); (2) green algae dominated, mixed foraminiferal wackestone–packstone microfacies (EMII); (3) ostracod, green algae and gypsum dominating mudstone–wackestone microfacies (EMIII); (4) algae and mixed foraminiferal wacke–packstone microfacies (EMIV); (5) *Nummulites* dominating mudstone–wackestone microfacies (EMV); (6) algal limestone, mudstone microfacies (EMVI); (7) *Assilina* bed wackestone–packstone microfacies (EMVII); (8) micritized large benthic foraminiferal wackestone microfacies (EMVIII); and (9) algal limestone, mudstone microfacies (EMIX).

### 3.2.1. Dolomicritic Foraminiferal Mudstone–Wackstone Microfacies (EMI)

On the basis of detailed petrographic evaluations, this microfacies is subdivided into two subfacies, as follows.

#### Dolomicritic Mudstone–Wackstone Subfacies

The first subfacies (Dolomicritic mudstone–wackestone subfacies) is dominantly comprised of dolomicritic limestone rock bodies with an average grain size of 0.05 mm. Micrite is partly to completely dolomitized in this microfacies. Bioclasts (with an average of 10%) are partly to completely micritized. The few identified fossils are *Discocyclina ranikotensis* (Figure 5a), *Elazigina dienii*, *Fabiania* spp. (Figure 5a), *Lockhartia* spp. (Figure 5b), *Pelatispira* and *Rotalia trochidiformis* (Figure 5c). Deep water agglutinated arenaceous foraminifera, *Kathina namalensis*, are also present, as well as a rare amount of *Nummulite* spp. A considerable amount of hematite (with an average of 6%) and pyrite (with an average of 4%) can also be observed in this subfacies. Spar (with an average of 3%) and carbonaceous material (with an average of 2%) are found in a minor amount. Four samples from the bottom of the Margalla Hill Limestone represent this subfacies (YMG1–YMG4).

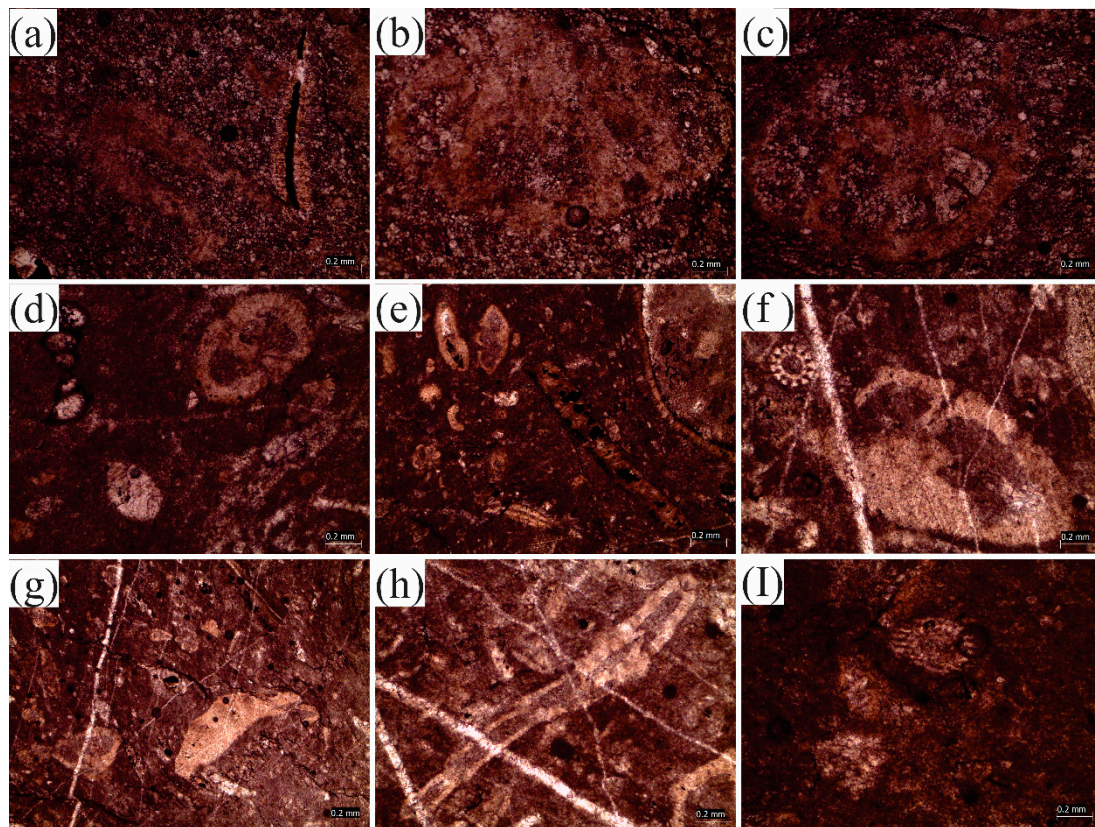


**Figure 5.** Photomicrographs showing (a) *Discocyclina* spp. on the right and *Fabiania* spp. on the left; (b) *Lockhartia* spp.; (c) *Rotalia trochidiformis*; (d) *Acervulinidae* spp. on the left and *Rotalia trochidiformis* on the right; (e) *Distichoplax biserialis* (coralline algae); (f) echinoid spine (*Echinothrix*); (g) *Quinqueloculina granulocostata* and calcified algae (*Vermiporella*); (h) *Ranikothalia nuttalli*; and (i) spatangoid spine algae.

#### Mixed Foraminiferal Wackstone Subfacies

This micritic wackestone subfacies is dominantly comprised of bioclasts (with an average of 40%). Bioclasts are found partly micritized in thin sections. Fossils identified are: *Assilina* spp., *Acervulinidae* spp. (Eocene) (Figure 5d), coralline algae, *Discocyclina* spp., *Distichoplax biserialis* (Figure 5e), echinoid spine (*Echinothrix*) (Figure 5f), *Eorupertia* spp., green algae, *Heterostegina*, *Lockhartia ramanae ten dam*, *Lockhartia daviesi*, *Lockhartia*

*tipper*, *Operculina* spp., *Orbitolites* spp., *Millioliidae* (*Quincoloculina*), *Quinqueloculina carinata* d'Orbigny, *Quinqueloculina granulocostata* (Figure 5g), calcified algae (*Vermiporella*) (Figure 5g), *Ranikothalia nuttalli* (Figure 5h), *Rotalia trochidiformis* and spatangoid spine algae (Figure 5I). Micrite is found as the second dominant constituent (with an average of 29%). Multiple cross-cutting and parallel calcite veins can also be seen with an average of 8% in this subfacies. Spar and hematite are observed with an average of 6% each, while dolomite and carbonaceous material are present with an average of 5% and 2%, respectively. Gypsum starts to appear in a minor amount (with an average of 1%) in this subfacies. This microfacies is represented by four thin sections (YMG5–YMG8).

**Interpretation:** This dolomitic limestone is dominantly comprised of unimodal-shaped crystals. Dolomite crystals range in shape from subhedral to anhedral. Crystal boundaries have planar contact with each other. These shapes and textures revealed the rock formation was subjected to low temperature (between 50–100 °C). Under low temperatures and constant Mg-rich fluid supply conditions, medium-grained subhedral–anhedral dolomite crystals are developed [23–26]. Medium–coarse crystals of dolomite can be observed sometimes in bioclasts. This resulted from the recrystallization of already formed dolomite, which eventually caused damage to the original depositional texture [27]. *Rotalia* spp. indicate a middle-Cuisian (early Ypresian) age [10]. An echinoid spine (*Echinothrix*) is identified in this microfacies. The echinoids largely influenced the coral reef's ecology [28–30]. After diagenesis of the shells of echinoderms, the high magnesium calcite ratio may be altered into low magnesium calcite. Echinoderms indicate deposition on a carbonate platform in a warm shelf setting where they are present with coral reefs, eventually facilitating carbonate mud production [31]. *Discocyclusina* spp. and *Pellatispira* spp. suggest a depositional site on a deeper portion of the carbonate platform [32]. Dascycladacean algae, such as *Vermiporella*, have not previously been reported in Eocene shelf carbonates [33]. The presence of *Vermiporella* and other calcified green algae indicates a photic and oxygenated zone in a shallow marine environment. Coralline red algae and other foraminifera, such as *Ranikothalia* spp., *Assilina* spp., *Millioliidae*, *Lockhartia* spp., *Orbitolites* spp., and *Rotalia* spp., indicate a relatively deep position of deposition on a carbonate platform [10]. This microfacies is found to be equivalent to FZ8 (restricted marine platform) of Flügel and Munnecke [34].

### 3.2.2. Green Algae Dominated, Mixed Foraminiferal Wackstone–Packstone Microfacies (EMII)

The second microfacies (green algae dominated, mixed foraminiferal wackstone–packstone microfacies (EMII) is recognized by the frequent abundance of calcispheres (*Vermiporella*) (Figure 6a), *Coccolitha orali* İnan, Dascycladacean green algae (Figure 6a), phylloid algae (Figure 6a), red algae (Figure 6b), *Salpingoporella melitae* Radoičić, Spatangoid spine, and a high amount of *Gymnocodiacea* green algae (Figure 6c). On the top portion of this microfacies, red algae (holothurian ossicles) start to appear in a minor amount. Other foraminifera are frequently observed and identified as: *Assilina leymyeri*, *Heterostegina* spp., *Holothurian* spicules (ossicles) (Figure 6d), *Idalina grelaudae* (Middle Eocene millioliidae) (Figure 6d), *Lockhartia haimei*, *Lockhartia prehaimei* (Figure 6e), *Lockhartia retinata*, ostracod (Figure 6f), Phylloid (Figure 6g), *Gymnocodiacea* (Figure 6g), *Pellatispira* spp. (Figure 6h), *Rotalia trochidiformis* (Leutitian age), *Saccamina grzybowskii* (Eocene foram) (Figure 6I) and *Textularia*. Crinoidea and echinoid spine are also observed. These bioclasts formed a predominant portion (with an average 50%) of this microfacies. Micrite, spar, and dolomite can be found with an average of 23%, 9%, and 6%, respectively. Hematite, carbonaceous material, pyrite, and gypsum gradually increase from base towards the top of this microfacies with averages of 2–3%, 1–2%, 2%, and 1–2%, respectively. Calcite is absent in the base and appears from the middle to the top of the microfacies with an average of 2% (Table 3). This microfacies is represented by four thin section samples (YMG9–YMG20).

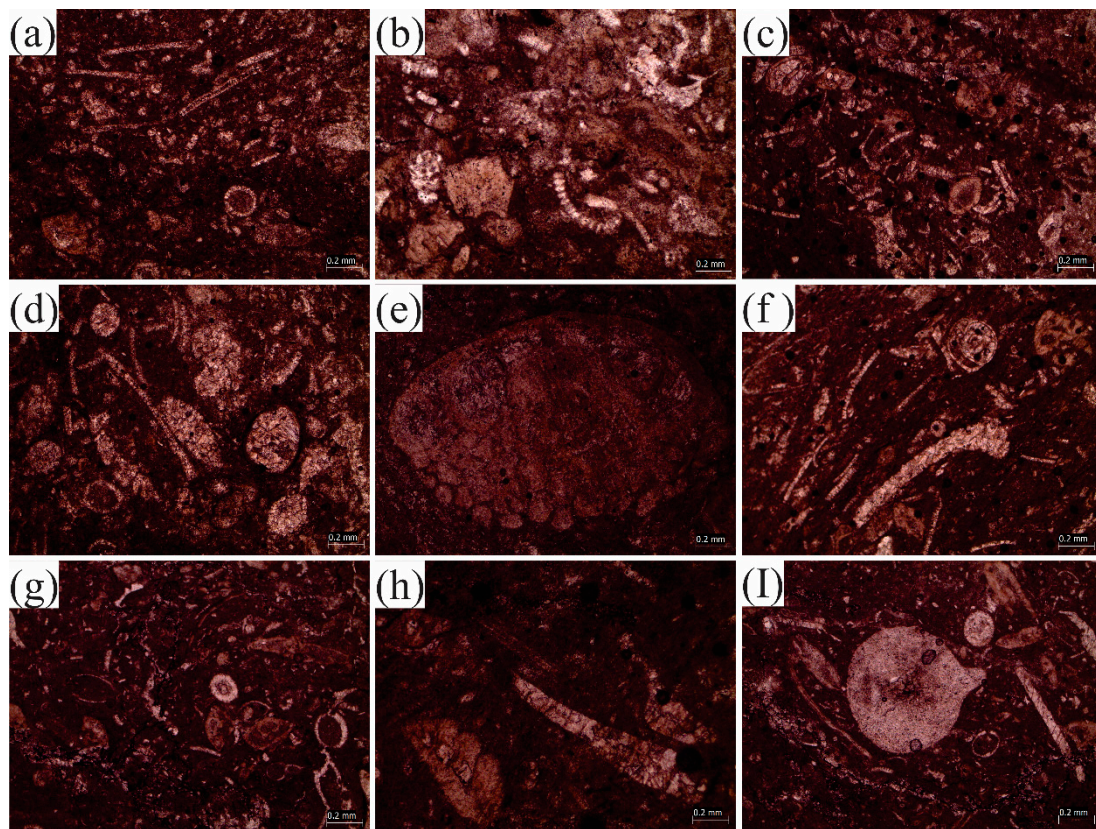


**Figure 6.** Photomicrographs showing (a) phylloid, dascycladacean and calcispheres algae; (b) mixed red and green algae; (c) Gymnocodiaceae; (d) holothurian spicules (ossicles) and *Idalina grelaudae* (Middle Eocene milliolid); (e) *Lockhartia praeahimeii*; (f) ostracod and green algae; (g) phylloid and gymnocodiaceae green algae; (h) *Pellatispira* spp. and phylloid algae; and (i) *Saccamina grzybowskii* (Eocene foram).

**Table 3.** An average mineralogical composition of the Early–Middle Eocene carbonate microfacies of Yadgaar Section.

Microfacies	Spar (%)	Micrite (%)	Bioclasts (%)	CM (%)	Pyrite (%)	Hematite (%)	Chert (%)	Gypsum (%)	Dolomite (%)	Calcite vein (%)	Deposition Site on Platform by Flügel and Munnecke
EMI	4	20	25	2	3	6	-	0.5	35	4	FZ8
EMII	11.5	25	55	1	2.5	3	-	2	7	2	FZ7
EMIII	4	57	19	2.5	1	6.5	-	1	8	1	FZ6–FZ5
EMIV	6.5	26	53	2	3	5	-	0.5	3	1	FZ5
EMV	-	62	11	2	3.5	4	-	1	15	1	FZ3
EMVI	-	21	3	19	4	7.2	1	2	38	7	FZ9A–FZ9B
EMVII	4	7	53	15	2	3	0.5	2	14	-	FZ6–FZ7
EMVIII	8	19	33	22	3	0.5	1	6	17	3	FZ7–FZ8
EMIX	-	38	3	19	1	0	3.5	1	20	107	FZ8

**Interpretation:** This microfacies displays a wide range of mixed bioclasts, from green algae species to larger foraminifers. Green algae (calcispheres, Dascycladacean, echinoid spine, Gymnocodiaceae, and phylloidal green algae) are identified in this microfacies. These

green algae indicate a very shallow depth, normally 5–15 m on a carbonate platform. The wide range of these algae indicates a highly oxygenated environment and a photic zone [8,35–37]. Some larger foraminiferans and broken ostracod shells, *Lockartia* spp., milliolid, and *Rotalia* spp., may be reworked from adjacent microfacies due to high energy wave action and deposited in this microfacies as a mixture of bioclasts. This microfacies is equivalent to FZ7 (open marine platform) [34].

### 3.2.3. Ostracod, Green Algae, and Gypsum Dominating Mudstone–Wackstone Microfacies (EMIII)

This microfacies is subdivided into three subfacies, listed as follows.

#### Ostracod, Coralline Algae, and Green Algae Dominated Mudstone–Wackstone Subfacies

This subfacies is identified by a frequent abundance of ostracods and green algae. However, fossils are partly or completely micritized and often replaced by hematite. Micrite is the dominant constituent of this subfacies (with an average of 61%). The abundance of bioclasts appeared comparatively low (with an average 15%). Microfossils identified are *Boueina marondei*, bryozoans, coralline algae (*Sporolithon* spp.) (Figure 7a), *Idalina grelaudae* (Middle Eocene milliolid) (Figure 6a), *Discocyclina* spp., echinoid spine, green algae (Dasycladacean, Salpingoporellamelitae Radoičić), *Fabiania* spp., filamentous shells of bivalves (Figure 7b), *Heterostegina* spp., *Lockhartia prehaimei*, *Lockhartia haimei*, nummulites, *Ocoarota orali* İnan, ostracod (Figure 7c), *Assilina* spp. (Figure 7d), *Quinqueloculina* and *Rotalia* spp. Dolomite starts to increase in this subfacies (with an average 7%). Hematite, spar, carbonaceous matter, pyrite, gypsum (Figure 7e), and calcite can be observed in minor amounts with an average of 1–6%. Four samples represent this subfacies (YMG21–YMG24).

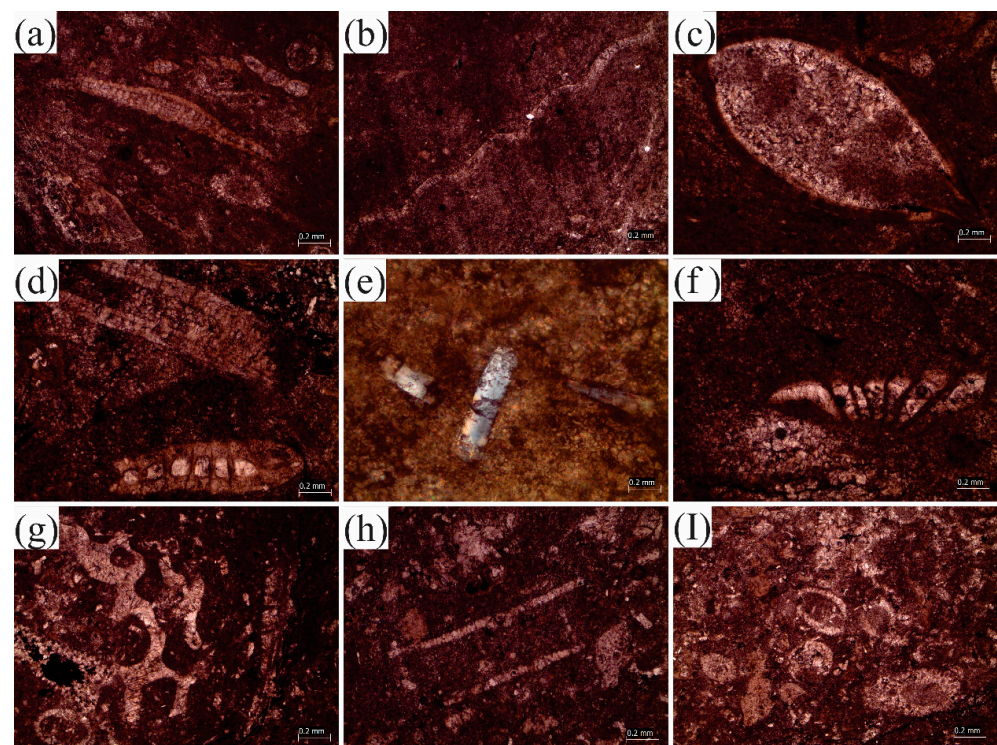


**Figure 7.** Photomicrographs showing (a) coralline algae and *Idalina grelaudae* (Middle Eocene milliolid); (b) filamentous shells of bivalves; (c) an ostracod; (d) *Assilina* spp.; (e) gypsum; (f) unidentified algal fossil; (g) algae; (h) Calcispheres green algae and Spatangoid spine algae; and (i) Dasycladacean green alga (*Cymopolia elongata*).

#### Gypsum Dominating Low Fossiliferous Mudstone–Wackstone Subfacies

This subfacies is identified on the basis of well-developed gypsum crystals (with an average of 2%). Micrite is found frequently, with an average of 53%. Small-sized

fossils are micritized and are observed at an average of 12%. *Assilina* spp., *Austrotrillina eocenica*, broken red algae, *Calcarina* spp., *Entogonia formosa*, *Idalina grelaudae* (Middle Eocene miliolid), *Lockhartia praehaimeii*, *Lockhartia* spp., unidentified algal fossil (Figure 7f), *Ocoarota orali* İnan, *Pellatispira madaraszi*, and *Ranikothalia* spp. Dolomite crystals start to appear considerably, with an average of 16%. Hematite is identified in the highest amounts, with an average of 9% in this subfacies. Spar, carbonaceous material, and pyrite can be observed in 5%, 2–3%, and 1%, respectively (Table 3). This subfacies is represented by four samples (YMG25–YMG28).

#### Green Algae Dominated Wackstone Subfacies

This subfacies is mainly comprised of green algae (Figure 7g), such as calcified algae (*Vermiporella*), spatangoid spine algae, calcisphere green algae (Figure 7h), and dasycladacean green algae (*Cymopolia elongate*) (Figure 7i). Other fossils are *Fabiania* spp., *Lockhartia* spp., *Lockhartia* spp., *Rotalia trochomiferous*, ostracods, and spatangoid spines. Fossils are highly micritized and species identification is hard. Micrite and bioclasts formed the dominant portions of the thin sections with an average of 57% and 30%, respectively. Hematite and spar are found in 5% and 3%, respectively. Carbonaceous material, pyrite, and calcite are observed in 3%, 1%, and 1%, respectively. This subfacies is represented by four thin sections (YMG29–YMG32).

**Interpretation:** Selective dolomite patches can be observed in the thin sections of this microfacies. Most bioclasts are observed to be prone to selective dolomitization. This type of dolomitization is associated with fine-grained, micritized allochem particles and their hard parts [23,38]. This may cause a lowering of the porosity values [39,40]. Coralline red algae's stratigraphic range is widely distributed and is mostly found in shallow water [41]. The co-existence of coralline algae and large benthic foraminiferans may indicate a 40–45 m (medium) water depth on a carbonate platform [42–44]. Corals are found in shallower areas as compared to sponges. They are found in association with marl or silty sandy environments with an abundance of benthic foraminiferans [45]. Corals and sponges are found in closely related environments adjacent to each other but with different environments ranging from shallow to moderately deep environments. Deep sea settings with high sea level rise may be indicated by the presence of these red coralline algae [46]. The presence of *Pellatispira*, *Heterostegina* spp., and *Discocyclusina* spp. suggests a deeper depositional environment in a carbonate platform [32]. This microfacies is equivalent to FZ6 (platform margin) and FZ5 (upper slope reefs and platform-margin reefs) [34].

#### 3.2.4. Algae and Mixed Foraminiferal Wackstone–Packstone Microfacies (EMIV)

This microfacies is subdivided into two subfacies, as follows.

##### Mixed Foraminiferal Micritized Packstone Microfacies

This subfacies is comprised of highly micritized bioclasts. However, the size and abundance of fossils are relatively larger than the adjacent subfacies. The bioclasts encountered in this subfacies were *Alveolina* spp. (Figure 8a), *Assilina* spp., *Austrotrillina eocenica* (Figure 8b), *Operculina subsalsa* (Figure 8b), crinoid ossicles, echinoid spines, green algae (Gymnocodiaceae, phylloid algae, and spatangoid spines) (Figure 8c), Eocene sponge (Figure 8c), *Idalina grelaudae* (middle Eocene miliolid) (Figure 8d), *Lockhartia haimeii*, *Lockhartia prehaimeii* (Figure 8e), *Lockhartia tipper* (Figure 8e), the miliolid (*Quinqueloculina*), ostracods, *Rotalia trochidiformis*, and spatangoid spines. Bioclasts are dominant in the thin sections and their average distribution is about 56%. Micrite, spar, and hematite are observed as 22%, 9%, and 5%, respectively. Dolomite, carbonaceous material, and calcite are found in 2%, 2%, and 1%, respectively. Four samples represent this subfacies (YMG33–YMG36).

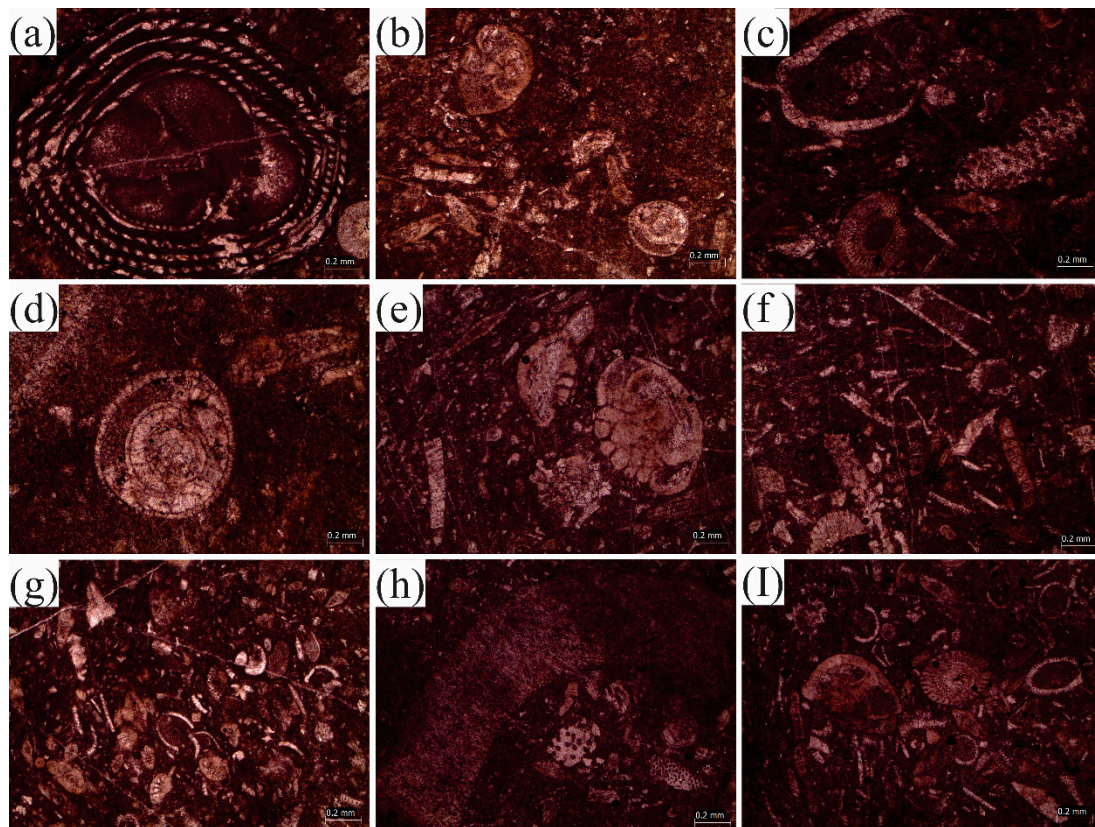


**Figure 8.** Photomicrographs showing (a) *Alveolina* spp.; (b) *Austrotrillina eocenica* on the right and *Operculina subsalsa* on the left; (c) Gymnocodacea in the bottom, ostracods in the top left, and sponge in the middle right; (d) *Idalina grelaudae* (Middle Eocene milliolid); (e) *Lockhartia prehaime* on the right and *Lockhartia tipperi* on the left; (f) Dascycladacean green algae and *Cymopolia elongata* on top; (g) high concentration of green algae; (h) *Fabiania* spp.; and (I) *Rotalia trochidiformis* and echinoid spine.

#### Mixed Green Algae and Broken Bioclastic Wackstone–Packstone Subfacies

This subfacies is identified on the basis of the special appearance of a mixture of fossils. This mixture is dominantly comprised of green algae and broken clasts of other large fossils (with an average 50%). Fossils identified are green algae (Dascycladacean, *Cymopolia elongate*, Gymnocodiacea, echinoid spines) (Figure 8f,g), *Assilina* spp., Eocene sponge, *Fabiania* spp. (Figure 8h), *Rotalia trochidiformis* (Figure 8I), *Idalina grelaudae* (Middle Eocene milliolid), unidentified algal fossils, *Lockhartia prehaime*, *Lockhartia tipper*, *Lockhartia retiata*, *Orbitolites* spp., ostracods, and sponges (Figure 8I). Micrite is found as the second-most abundant behind fossil fragments, with an average 30% in this subfacies. Pyrite, hematite, spar, dolomite, carbonaceous material, and calcite are 5%, 4%, 3%, 2%, and 1%, respectively. Four samples represent this subfacies (YMG37–YMG40).

**Interpretation:** Selective dolomitization in packstone–grainstone may facilitate dissolution, which can enhance porosity and reservoir characteristics [23,47]. Selective dolomitization can be observed in this microfacies. Autochthonous sponges from the Eocene sequence of the Yadgaar section have been reported for the first time. Most of these Eocene sponges are in broken fragments. The skeletons of sponges seem to be micritized, which indicates a diagenetic effect (neomorphism) on them. The association of sponges with coral indicates a relatively deep shelf area. However, the absence of coral and the appearance of sponges are indicative of shallower water depth [45]. Furthermore, broken sponge pieces indicate a moderate–high energy upper slope outer platform environment [48]. This also indicates a deep environment; however, the depth was not enough to provide a fully reduced paleogeographic constraint [45]. Ostracods characterize cold marine and deep

environments [49]. This microfacies represent a wide facies belt and is equivalent to FZ5 (upper slope reefs and platform-margin reefs) of Flügel and Munnecke [34].

### 3.2.5. Nummulites Dominating Mudstone–Wackstone Microfacies (EMV)

This mudstone-wackstone microfacies is dominantly comprised of micrite material (with an average 62%). Bioclasts are partly to completely micritized (with an average 11%). Fossils identified are *Assilina* spp. (Figure 9a), gastropods and geopetal infillings (Figure 9b), *Lockhartia* spp., *Nummulites* spp. (Figure 9c,d), *Operculina* spp. (Figure 9e), *Ranikothalia* spp., and *Rotalia trochidiformis* (Figure 9f). Dolomitization is often found in the form of dolomite patches (Figure 9g) in the thin sections (with an average of 15%). Alteration of blocky cement into dolomite has been observed (Figure 9h). The changing of micrite into dolomite is obviously seen in this microfacies (Figure 9I). Carbonaceous material (with an average of 2%) and hematite (with an average of 4%) have commonly replaced fossils. Pyrite, gypsum, and calcite can also be seen with averages of 4%, 1%, and 1%, respectively (Table 3). This microfacies is represented by four samples (YMG41–YMG44).

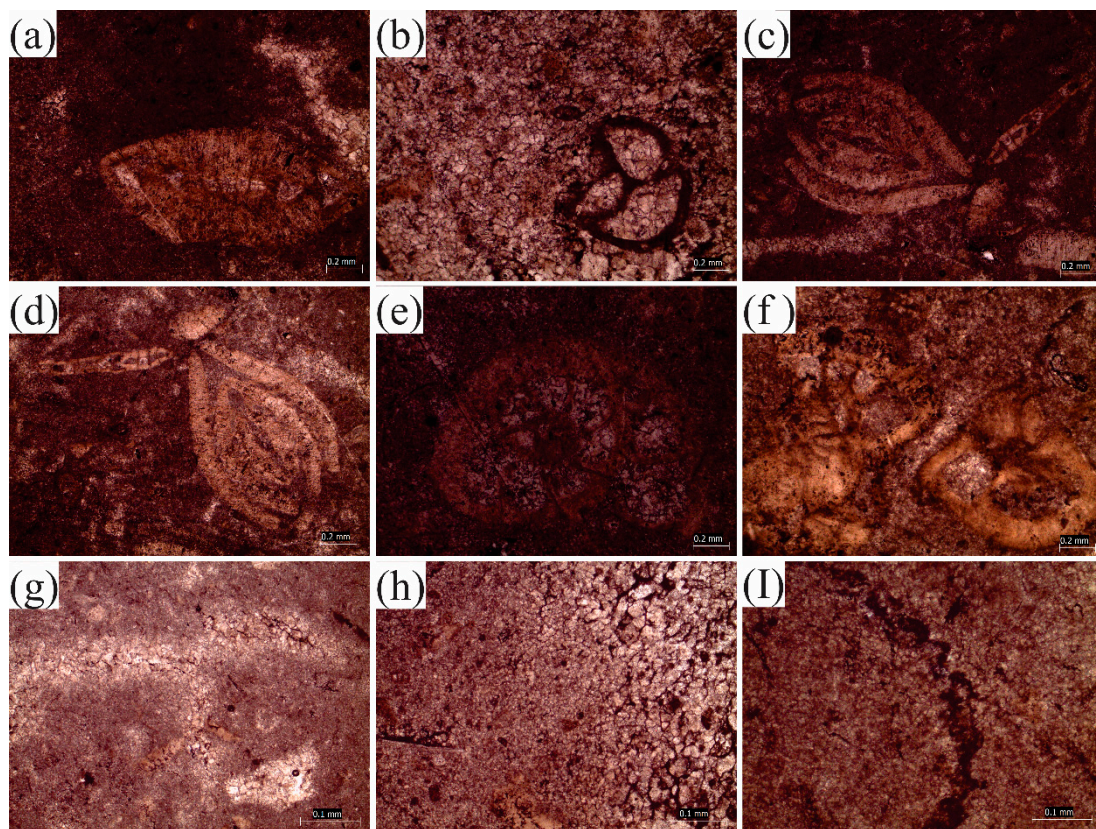


**Figure 9.** Photomicrographs showing (a) *Assilina* spp.; (b) gastropods and geopetal infillings; (c,d) *Nummulites* spp.; (e) *Operculina* spp.; (f) *Rotalia trochodeformis* on the left and *Lockhartia tipperi* on the right; (g) a dolomite patch; (h) blocky cement changing into dolomite; and (I) micrite changing into dolomite.

**Interpretation:** Gastropods indicate normal salinity and a shallow-marine shelf environment. The presence of *Nummulites* spp. characterize a subtidal environment and depth ranges from 20 to 130 m with the precipitation of lime mud [50]. *Operculina* spp. indicated the 6–15 m depth but typically dominates in the zone of 30–54 m. This also signifies the presence of a depositional site in low energy and medium light intensity in a reef slope [51]. Sometimes these types of deposits resulted from turbidites. *Operculina* spp. are identified in this microfacies. Benthic foraminifera, such as *Assilina* spp., *Operculina* spp., and *Ranikothalia* spp., indicate a depositional site in a lagoon, reef setting, or inner

ramp environment in the Tethys ocean [52,53]. These Early–Middle Eocene microfossils found in this microfacies indicate close association with reefs in a lagoon environment. This microfacies is equivalent to FZ3 (toe-of-slope apron deep shelf margin) of Flügel and Munnecke [34].

### 3.2.6. Algal Limestone and Mudstone Microfacies (EMVI)

This microfacies is uniquely identifiable by the appearance of algal limestone. Algae and other bioclasts are completely micritized and unidentifiable. Micrite is further dolomitized (Figure 10a) in this microfacies. Dolomite is observed at an average of 38%, while micrite forms 21% of the thin sections. Carbonaceous material is also found at an average of 20% in this microfacies. Cross-cutting calcite veins (7%) and pyrite cubes (1%) are also present. Hematite, bioclasts, gypsum (Figure 10b), pyrite (Figure 10c), and chert (Figure 10d) can be observed with averages of 7%, 3%, 2%, and 1%, respectively (Table 3). This microfacies is represented by four samples (YCF1–YCF4).

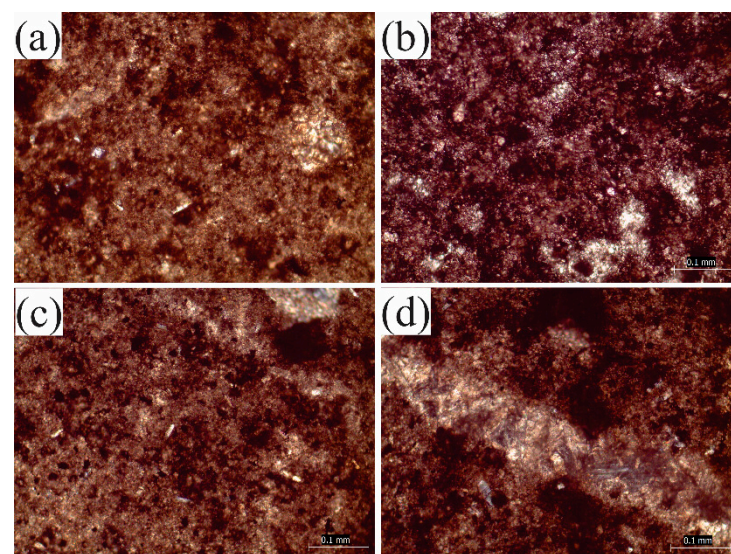


**Figure 10.** Photomicrographs showing (a) dolomitized bioclast and gypsum; (b) gypsum, hematite and micrite; (c) gypsum and pyrite; and (d) chert.

**Interpretation:** Gypsum (an evaporitic sulfate mineral) is often found in lagoon conditions associated with methane hydrate settings [54,55]. Fibrous gypsum is comprised of two main forms, a) satin spar and b) selenite [56], and is found in shallow marine limestone and shale. In evaporitic conditions where carbonate rocks react with acid sulfate, they will precipitate gypsum [57]. Gypsum is also formed by the oxidation of iron sulfide (pyrite). Recent studies have revealed a direct relationship between methane hydrate sediments, gypsum, and pyrite. The sulfate–methane transition zone often facilitates the precipitation of authigenic gypsum [56]. The coexistence of both gypsum and pyrite is tricky to explain, depending on whether the conditions are anoxic or oxic. By the activity of sulfide oxidizers, oxidized pyrite is converted into sulfate in oxic conditions, resulting in the formation of gypsum. In a sedimentary environment, these settings are called marine methane hydrate settings [58]. The connection between methane-bearing sediments and mineralization is still unclear. Gypsum is largely found to be associated with methane hydrate settings in the southwest African Margin, the Bay of Bengal, the South China Sea, and the eastern North Pacific Ocean [55]. However, in anoxic conditions, the process is reversed where sulfate-reducing bacteria convert the gypsum into pyrite [59]. Gypsum precipitation likely largely occurred after considerable and rapid evaporation, and this was presumably linked with a reduction in the size of the lake. However, the lake’s bottom was still anoxic, which facilitated pyrite precipitation [54]. Sulfide/sulfate anions and Ca/Fe cations in the solution can precipitate gypsum and pyrite [56]. The pyrite and gypsum

phases are tightly associated. In fresh and shallow waters, larger benthic foraminifera are absent. Their presence occurs only in relatively deep waters [60]. This microfacies is equivalent to FZ9A (arid near-coast evaporitic platforms) to FZ9B (humid near-coast brackish regions) of Flügel and Munnecke [34].

### 3.2.7. Assilina Bed Wackstone–Packstone Microfacies (EMVII)

In this microfacies, *Assilina* spp. are more abundant than the other microfossils. The size and abundance of fossils is highest among all the microfacies (with an average of 53%). This microfacies is also comprised of a high amount of carbonaceous material, with an average of 15%. Micritization and dolomitization effects are also seen in thin sections. Dolomite can be found with an average of 14%, while micrite can be observed with an average of 7%. Stylolites are frequently observed in parallel to the bioclasts. Fossils are mostly *Assilina* spp. and nummulites (Figure 11a–c), while some coralline algae (Figure 11d), unidentified algal fragments, *Discocyclus ranikotensis* (Figure 11e), *Discocyclus zindaperensis* (Figure 11f,g), coralline algae, and *Rotalia trochidiformis* (Figure 11h,i) can be identified. Hematite, spar, gypsum, pyrite, and chert are found with averages of 3%, 4%, 2%, 2%, and <1%, respectively (Table 3). This microfacies is represented by eight samples (YCF5–YCF12).

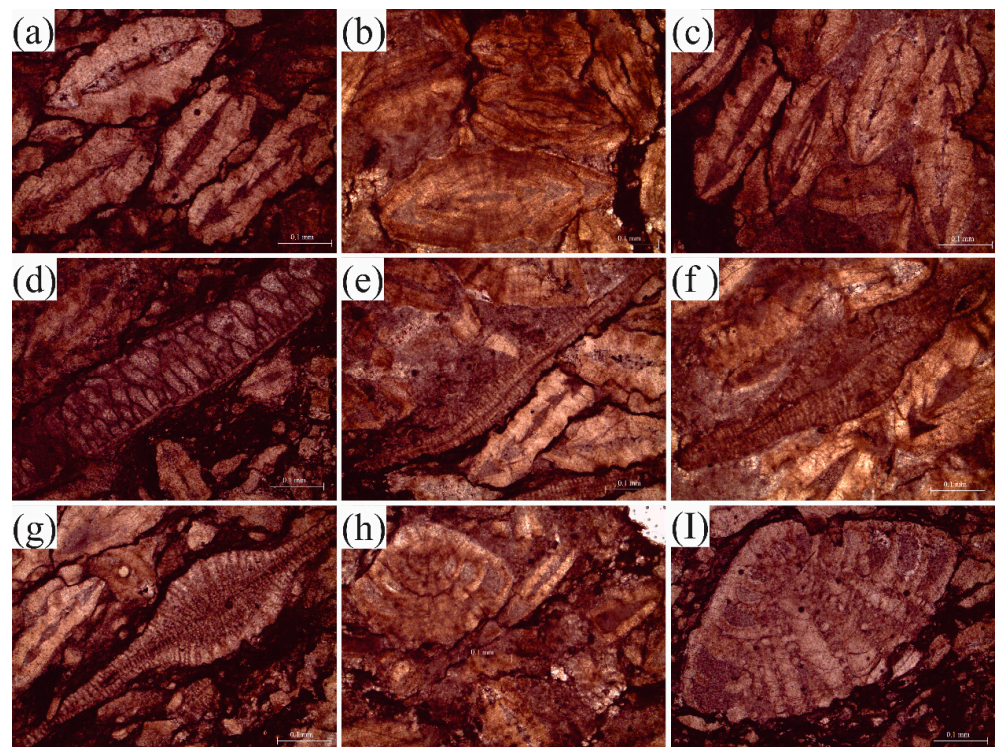


**Figure 11.** Photomicrographs showing (a) *Assilina* in the center to the right and *Nummulites* spp. on top; (b,c) *Assilina* spp.; (d) Coralline algae; (e) *Discocyclus ranikotensis* in the center and *Assilina* spp. on the right; (f,g) *Discocyclus zindaperensis* in the center; and (h,i) *Rotalia trochidiformis*.

**Interpretation:** A high abundance of *Assilina* spp. (preferably called the *Assilina* bed) may indicate a highly favorable salinity range and environmental depth for the continuation of species reproduction [61]. This can cause a high abundance of *Assilina* species in the microfacies. Larger foraminifera and *Orthophragminids*, especially *Discocyclus* spp., along with *Nummulites* spp. and *Assilina* spp., indicate deposition in the photic zone of carbonate ramp settings [61,62]. This microfacies is equivalent to FZ6 (platform-edge and platform sand shoals) to FZ7 (platform interior–normal marine (open marine)) of Flügel and Munnecke [34].

### 3.2.8. Micritized Large Benthic Foraminiferal Wackstone Microfacies (EMVIII)

This is a highly micritized microfacies in which large bioclasts are almost completely micritized. Micritization is intense enough to make the species unidentifiable (Figure 12a). However, very few bioclasts can be recognized in the middle–top portion as *Alveolina* spp. (Figure 12b–d), *Assilina* spp., *Nummulites* spp. and *Assilina* spp. (Figure 12e,f), *Azzarolina daviesi*, *Lockhartia* spp., miliolid, *Operculina* spp., ostracods, and *Rotalia* spp. (Figure 12g). Bioclasts are abundantly found with an average of 32% in this microfacies. Dolomite and carbonaceous material are also found in large quantities, with averages of 17% and 13%, respectively. Micrite, spar, gypsum, calcite, pyrite, and chert (Figure 12h) were observed in 19%, 8%, 4%, 3%, 2%, and 1%, respectively (Table 3). Bioclasts are found to be replaced by carbonaceous material (Figure 12i). This microfacies is represented by four samples (YCF13–YCF24).

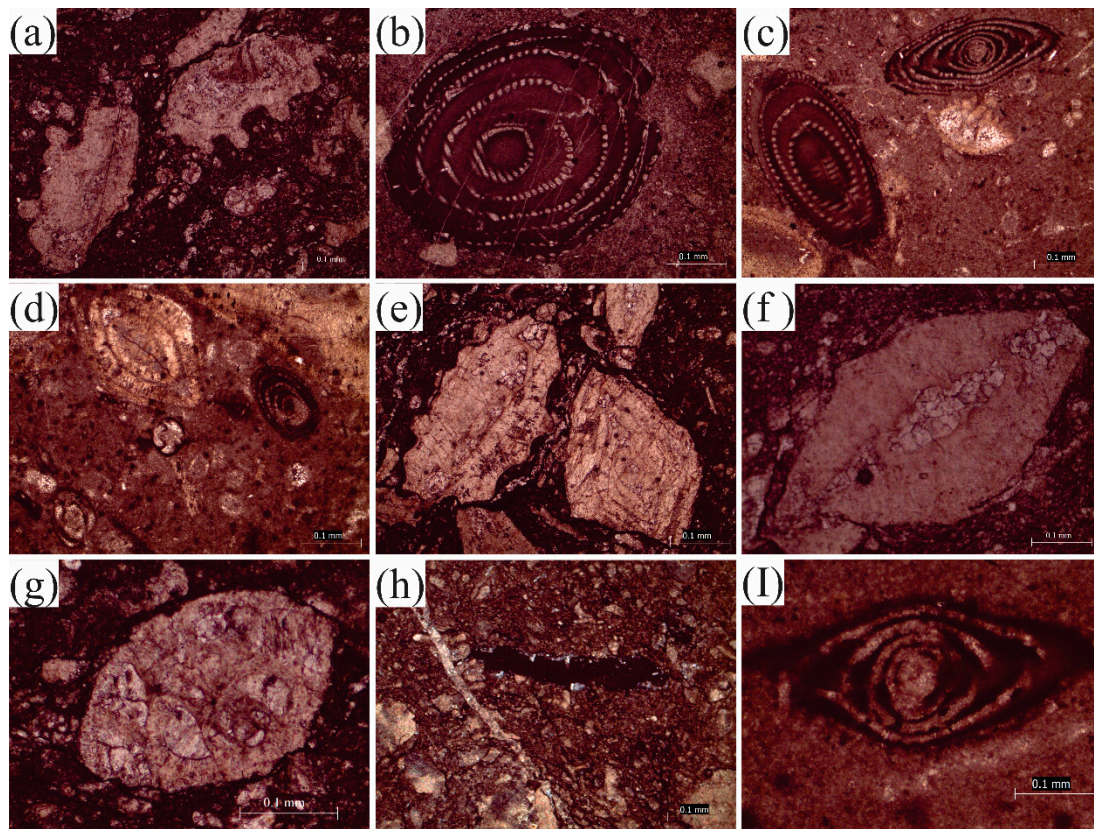


**Figure 12.** Photomicrographs showing (a) micritized bioclasts; (b,c) *Alveolina* spp., (d) *Nummulites* spp. on the left and *Alveolina* spp. on the right; (e) *Assilina* spp. on the left and *Nummulites* spp. on the right; (f) micritized *Assilina* spp.; (g) *Rotalia trochodiformis*; (h) carbonaceous material and chert replacing bioclast; and (i) *Nummulites* is replaced by carbonaceous material.

**Interpretation:** The presence of *Alveolina* spp., *Nummulites* spp., and *Assilina* spp. with moderate energy conditions, indicates inner ramp settings but with a slight increase in depth relative to where the previous microfacies were likely deposited [61]. *Nummulites* spp. are normally found in relatively deep settings [60]. This association of microfauna is found in the distal inner ramp area. This is a high energy, current-dominated environment close to fair weather wave base (FWWB). *Operculina* spp. along with *Nummulites* spp. are also indicative of an increase in water depth [61]. The large quantity of *Nummulites* indicates distal inner ramp to mid-ramp environments. This indicates a high-energy environment close to FWWB. This microfacies is equivalent to FZ7 (platform interior–normal marine–open marine) to FZ8 (platform interior–restricted) of Flügel and Munneke [34].

### 3.2.9. Algal Limestone and Mudstone Microfacies (EMIX)

The top microfacies of the Early–Middle Eocene carbonate sequence of the Yadgaar section is comprised of algal limestone (Figure 13a). Micrite is the dominant constituent with an average of 38%. Fossils are partly to completely micritized as we move towards the upper contact of the microfacies (with an average of 19%). Only very few *Alveolina* spp. (Figure 13a), green algae (Figure 13b), *Lockhartia* spp., *Nummulites* spp. (Figure 13c), miliolids and ostracods (Figure 13d) can be distinguished in this thin section study. The majority of fossils are completely micritized and unidentifiable. Dolomite crystals are abundantly found in this microfacies with an average of 20%. Calcite, bioclasts, chert (Figure 13e–h), gypsum, pyrite (Figure 13e–h), and hematite (Figure 13I) were observed with averages of 13%, 3%, 4%, 1%, 1% and <1%, respectively (Table 3). This microfacies is represented by four samples (YCF25–YCF32).

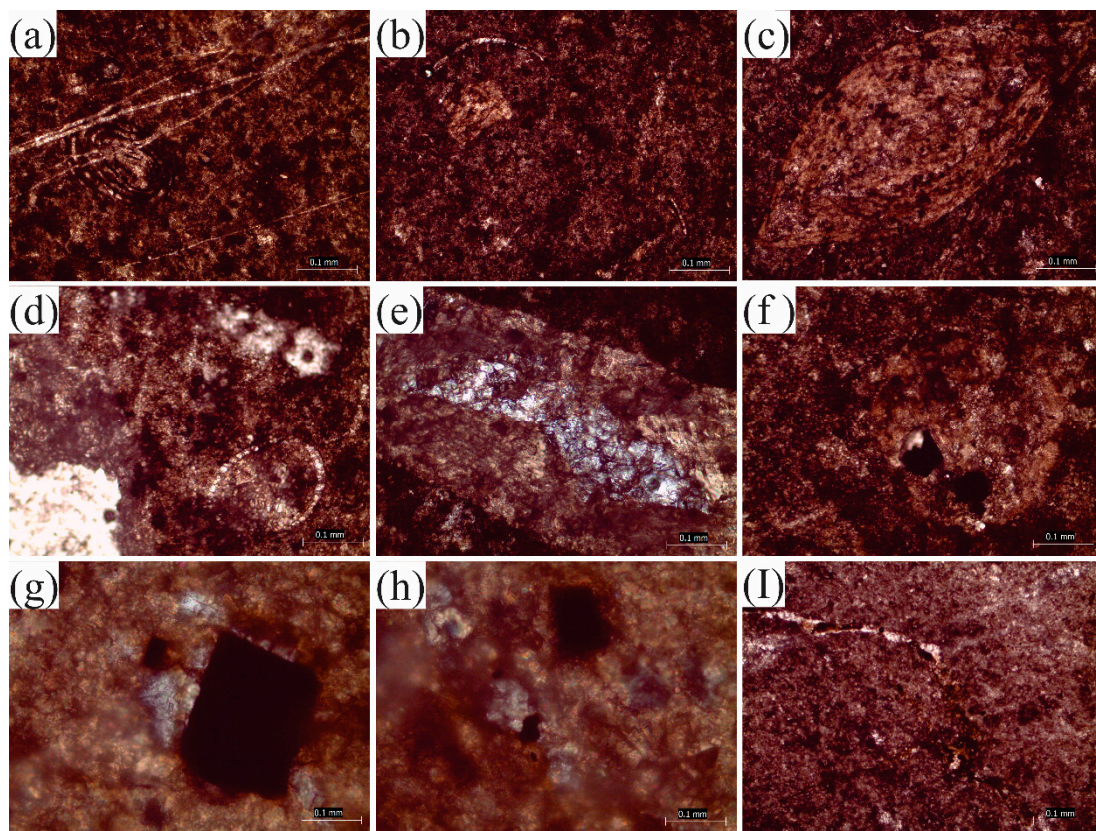


**Figure 13.** Photomicrographs showing (a) algal limestone and *Alveolina* spp.; (b) broken clasts of green algae; (c) *Nummulites* spp.; (d) an ostracod; (e) chert in calcite vein; (f–h) pyrite cubes in black; and (I) a hematite vein.

**Interpretation:** *Alveolina* spp. is compatible with a variegated salinity-temperature range and indicates inner ramp settings [63]. On a carbonate platform, it is distributed over a wide shallow water platform area <35 m [64]. This area is specifically just below the fair weather wave base in a high energy environment [65]. However, *Alveolina* spp. can also be found at a depth of up to 60 m in the fore-reef of a deep lagoon environment [66]. In the Eocene, *Alveolina* spp. associated with miliolids is typical of shallow water vegetative substrate in a sandy/sea grass environment [60,67–69]. This can be confirmed by the presence of chert in this microfacies, which comes from high water wave action. This indicates inner ramp settings (Figure 13e). The presence of *Alveolina* spp. in this uppermost microfacies indicates a Bartonian age and deposition in a deeper portion of the shallow marine platform [32]. This microfacies is equivalent to FZ8 (platform interior–restricted) of Flügel and Munnecke [34].

### 3.3. Depositional Environment

The Yadgaar Section lies on the margins of the Cenozoic Tethys Ocean. A comprehensive study of Paleocene–Oligocene rocks of the Yadgaar Section can reveal the depositional environment of rocks during the mature development and the closing stage of the Cenozoic Tethys Ocean. These rock formations include Lockhart Limestone of Late-Paleocene, Margalla Hill Limestone, and Chorgali Formations of Early–Middle Eocene, as well as Kuldana Formation of Middle Eocene–Early Oligocene age. A petrological study of the Late Paleocene Lockhart Limestone reveals its depositional environment as a shallow shelf carbonate platform, typically from the platform margin to the toe of the slope and slope areas [9]. This study indicated that shallow marine platform carbonates were deposited in the final phase of transgression–regression events during the Early–Middle Eocene age. These deposits are represented by the Margalla Hill Limestone and the Chorgali Formation in the UIB [8]. Detailed microfacies studies based on the textural and benthonic foraminiferans revealed their depositional environments on the carbonate platform (Figure 14). Early–Middle Eocene carbonates were categorized as EM-I–IX, belonging to the restricted-marine platform, open-marine platform, platform-edge and platform sand shoals, toe of slope and slope, arid near-coast evaporitic platforms, humid near-coast brackish regions, platform-edge and platform sand shoals, open-marine platform, open-marine platform, restricted-marine platform, and restricted-marine platform areas, respectively. These microfacies are found to be equivalent to the FZ8, FZ7, FZ6–5, FZ5, FZ3, FZ9A–FZ9B, FZ6–7, FZ7–FZ8 and FZ8 (Figure 14b) microfacies of Flügel and Munnecke [34]. The closing stage of the Cenozoic Tethys Ocean is marked by the deposition of the Middle Eocene–Early Oligocene Kuldana Formation. A detailed study on the Kuldana Formation indicated a transitional environment from deltaic to continental because of the presence of limestone lenses in the base and sandstone/shale alternations in the Yadgaar Section [8].

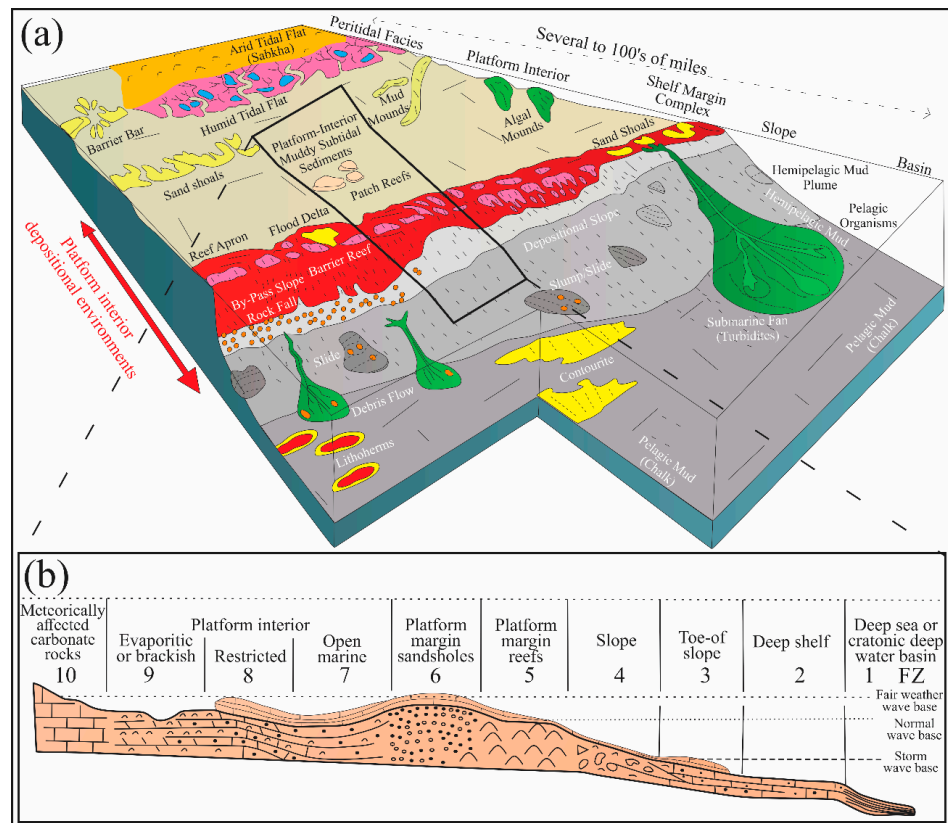


**Figure 14.** (a) Figure illustrating a generalized carbonate platform with associated environments. The rectangle corresponds to (b). (b) Depositional model of Early–Middle Eocene carbonate rock microfacies on specific zones of the carbonate platform [34].

### 3.4. Reservoir Characterization

#### 3.4.1. Diagenetic Impact

Early–Middle Eocene carbonate rocks are comprised of well-developed to fused nodular limestone and shales in the Yadgaar Section. To understand diagenetic effects on the carbonate Formations, eight samples of limestone and four samples of shale were collected from the base, middle, and top of the section for SEM analysis (Figure 15a–f). Light grey colored nodular limestone beds are present in the base and middle portions, while fused nodular limestone and shale are present in the top portion of the deposits in the study area deposits.

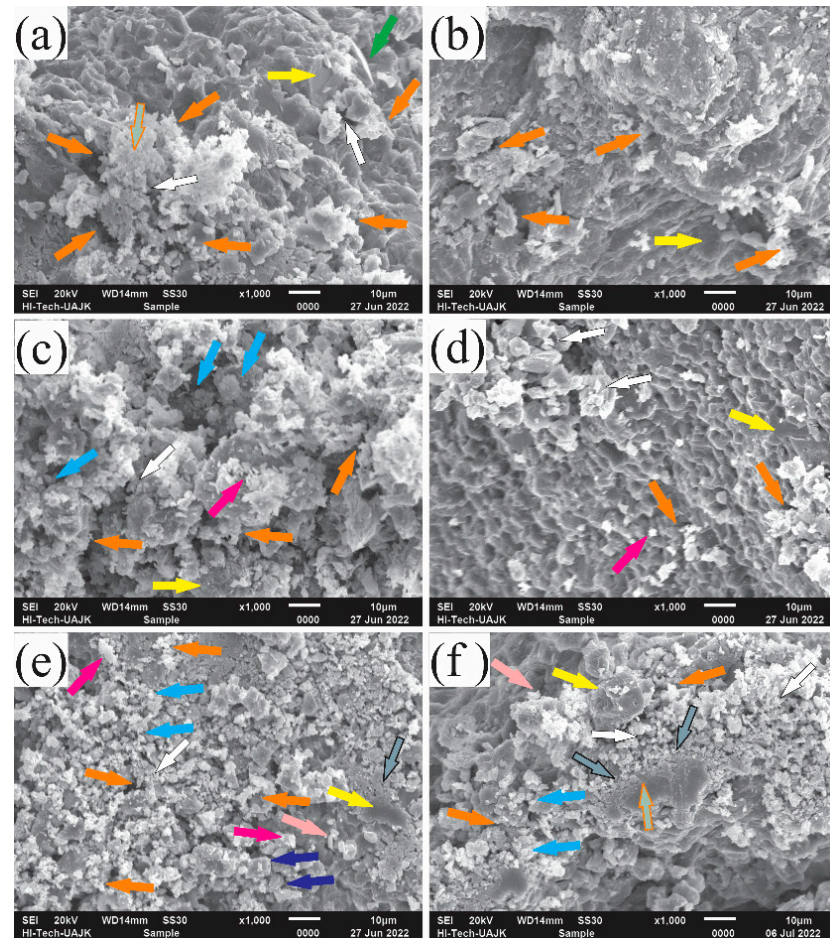


**Figure 15.** SEM image of shale and limestone samples from Early–Middle Eocene strata. (a,b) Images of the samples obtained from the base of the section; (c,d) Images of the samples taken from the middle of the Margalla Hill Limestone; (e,f) Images denote samples obtained from top of Margalla Hill Limestone. Yellow arrows denote calcite crystals, indigo blue arrows denote dolomite crystals, orange–brown arrows denote drusy cement, white arrows denote blocky cement, sky blue arrows denote rim cement, light grey arrows with a red outline denote compacted illite, indigo arrows with a red outline denote montmorillonite clay, and black arrows with red outline denote chert grains as found by Prothero and Schwab [70]. Moreover, green arrows denote a fibrous column of calcite, light pink arrows denote mosaic (drusy) dolomite cement, silver arrows with a black outline denote granular cement, and dark purple arrows denote dog tooth calcite crystals as found by Flügel and Munnecke [34].

SEM evaluations of the limestone (Figure 15a) and shale (Figure 15b) revealed the presence of first-generation drusy cement dominating throughout the Early–Middle Eocene deposits. In the Early–Middle Eocene deposits (Margalla Hill Limestone), first-generation cement is recognized by the presence of drusy cement. This shows the presence of the

first stage of post-depositional diagenesis (eogenetic) in the deposits. However, as shown in Figure 2, a minor occurrence of second and third generation cement was observed by the presence of blocky and rim cements, respectively. This demonstrates that mesogenetic and telogenetic diagenesis occurred here. The top section is comprised of middle Eocene strata (Chorgali Formation) (Figure 2), which possess an abundance of second-generation cements by the presence of blocky cement in the base, which starts to decrease towards the middle of the stratigraphic sequence. Meanwhile, first generation drusy cement again starts to increase towards the top of the section. In the middle Eocene strata, third generation rim cements are rarely found in the middle portion of the carbonate deposits.

Based on these results, our study found a greater abundance of cementation and other alterations that occurred during eogenesis compared to during later stages of diagenesis. However, in the middle part of the section (Figure 2), the grade of diagenesis slightly increased, which is revealed by the presence of mesogenetic and telogenetic cements of the-post depositional diagenesis. The minor presence of smectite, calcite crystals, chert, compacted illite, compacted montmorillonite, dog tooth calcite, dolomite, fibrous column of calcite, granular cement, montmorillonite clay, mosaic drusy dolomite, and radiaxial fibrous cement can also be observed in the SEM analysis (Figure 16).

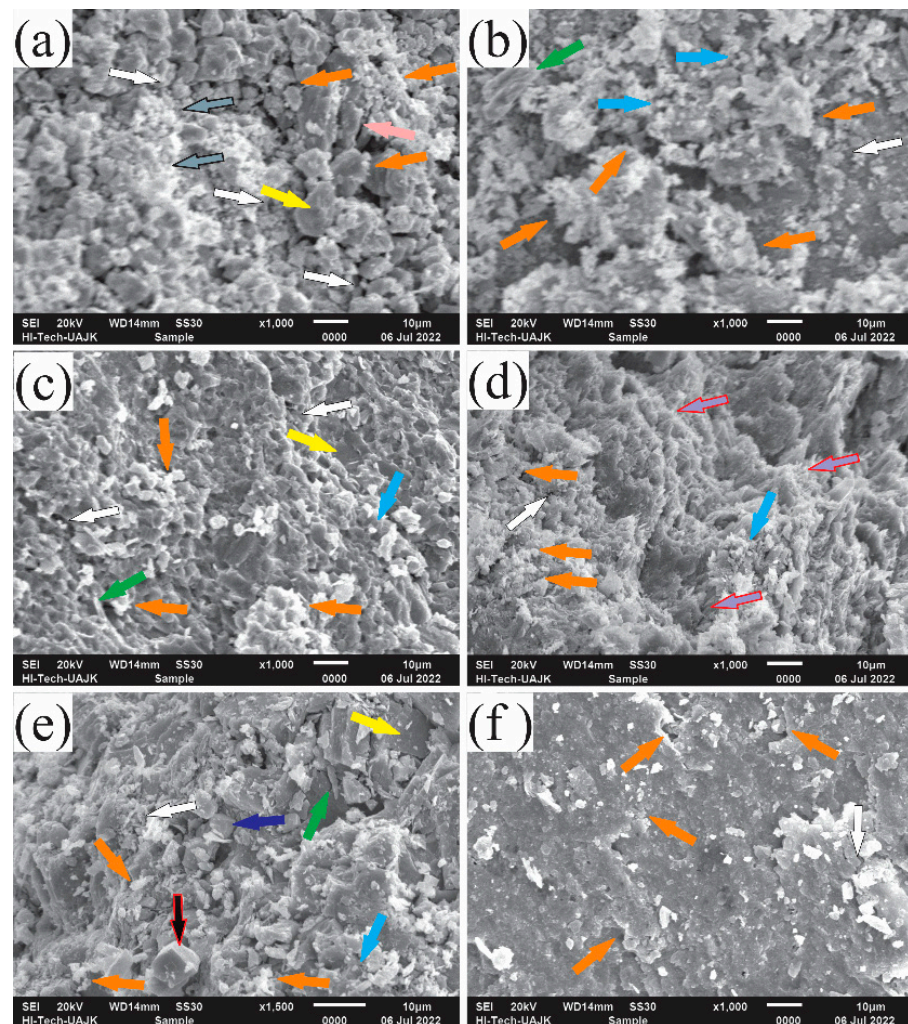


**Figure 16.** SEM image of shales and limestone samples from the Middle Eocene Chorgali Formation. (a,b) Images of the samples obtained from the base of the Chorgali Formation; (c,d) Images of the samples taken from the middle of the Chorgali Formation; (e,f) Images denote samples obtained from top of the Chorgali Formation. Refer to the caption of Figure 15 above for an explanation of the arrow colors.

### 3.4.2. Porosity Types and Reservoir Characteristics

From the base to top in Figure 17, the first microfacies (EMI) possesses a dominant presence of channel (Ch) type porosity along with little occurrence of channel (Ch), vuggy (Vg), and fenestral (Fe) pore types (Figure 17a). Image J software’s image threshold enhancement technique calculates the presence of 10% porosity in this microfacies (Figure 17a). The second microfacies (EMII) is composed of nearly equal amounts of vuggy (Vg), fractured (Fr), and moldic (Md) porosity (Figure 17b). The porosity calculated in this microfacies is 8%. The third microfacies (EMIII) is comprised of only fracture (Fr) and shelter (Sh) type porosities (Figure 17c). The calculated porosity in this microfacies is 10%. Vuggy (Vg) and fenestral (Fe) type porosities are also observed in the fourth microfacies EMIV (Figure 17d). The calculated porosity in this microfacies is 5%.

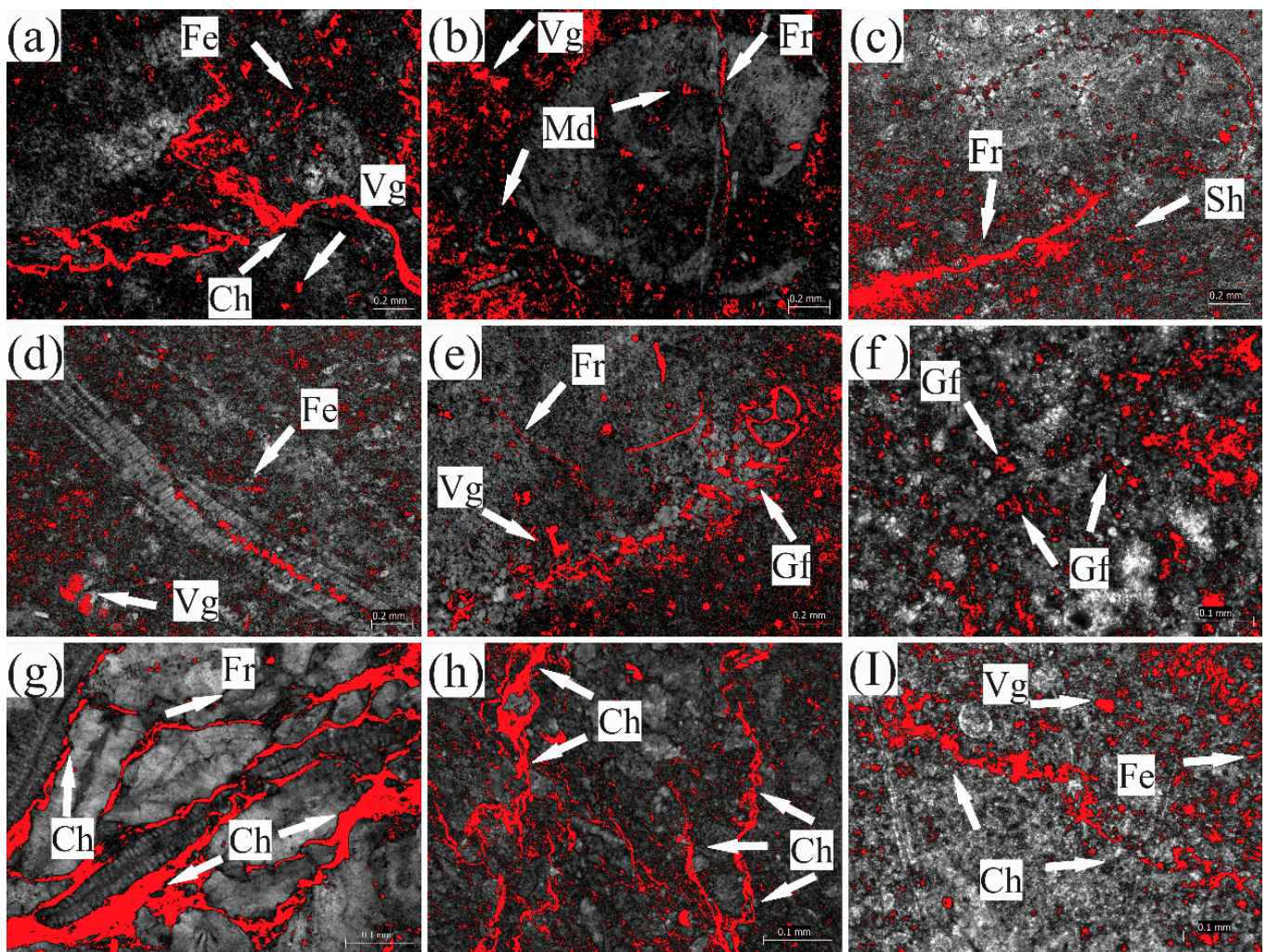


**Figure 17.** The image threshold enhancement technique in Image J software calculates porosity and reveals pore type for all microfacies of the Early–Middle Eocene rocks. (a–i) EMI, EMII, EMIII, EMIV, EMV, EMVI, EMVII, EMVIII, and EMVIX, respectively. Abbreviations of the porosity types shown in the figures: Fe, Fenestral; Ia, Intraparticle; Sh, Shelter; Vg, Vuggy; Ch, Channel; Gf, Growth Framework; Md, Moldic; and Fr, Fracture pore types.

An increase in porosity values has been noted as moving towards EMV (Figure 17e). The average porosity value for this microfacies was determined to be 10% (Figure 9c,d). This microfacies shows that vuggy (Vg) and growth framework (Gf) porosities are most common (Figures 9c and 16e), while fracture (Fr) porosity is less common. EMVI depicted only the growth framework (Gf) type of porosity, with a porosity value of 7% (Figure 17f).

In EMVII, the highest amount of porosity (15%) has been noted (Figure 17g). Frequent amounts of channel (Ch) and fracture (Fr) types of porosities can be observed clearly. The eighth microfacies (EMVIII) also displayed a higher porosity value of 11% (Figure 17h). However, only the channel (Ch) type porosity is observed in this microfacies. At the top of the Early–Middle Eocene carbonate rocks, strata comprising the ninth microfacies (EMIX) display channel (Ch), fenestral (Fe), and vuggy (Vg) types of porosities. This microfacies possesses 9% porosity (Figure 17i). The calculated average porosity from all microfacies of the Early–Middle Eocene carbonate strata in the Yadgaar Section is 7.4%.

Fracture and moldic types of porosities reveal the presence of early diagenetic effects such as the eogenetic alterations. They possess a low porosity but a high permeability range in shelf carbonate rocks, meaning they are of high reservoir quality [71,72]. Vuggy, fracture, and moldic porosities reflected within these sediments indicate they are favorable strata in terms of reservoir potential [72,73]. Fenestral porosity is associated with meteoric diagenesis. It can coexist with microfacies related to packstone, dolomitization, and dolomudstone [72]. The quality of a reservoir mainly depends on permeability, which is enhanced by the processes of dolomitization and de-dolomitization [74]. Channel type porosity is dominantly observed in thin sections of most microfacies. This type of porosity is likely to increase the permeability and reservoir quality. It is developed due to chemical dissolution in high energy conditions associated with diagenetic compaction [71,72,74]. Diagenetic features including fractures, channels, and dissolution are indications of tectonic forces exerted on the rocks after their formation [9,26,38,75]. In general, petrological observations, fracture, channel, growth framework, and moldic type porosities highly facilitate interconnecting pores, creating high permeability. The occurrence of all these types of porosities in the Early–Middle Eocene carbonate rocks of the Yadgaar Section is a positive signature of high reservoir quality.

#### 4. Conclusions

On the basis of field, petrographic, and SEM analysis, we have drawn the following conclusions. Early–Middle Eocene carbonate deposits of the Margalla Hill Limestone and the Chorgali Formation are found in the Yadgaar Section. Field observation and petrographic studies revealed nine microfacies (EMI–EMIX) within these deposits. Detailed paleontological and petrological studies indicate that these microfacies are deposited in the restricted marine (platform interior), open marine platform, platform edge, platform margin reef, toe of the slope apron, arid-humid platform interior, platform edge, open marine platform interior, and restricted marine platform interior, respectively, of the Ceno-Tethys Ocean. Benthic foraminifera microfossils revealed that these microfacies were deposited in the Early–Middle Eocene period in the Ceno-Tethys Ocean. Microfossils, including algae and foraminifera, as well as the presence of gypsum crystals, indicate shallow marine methane hydrate settings in complex lagoon conditions. Most of the microfacies (EMI–EMVI) from the base to upper-middle of the section were deposited in the shallow marine, oxygenated, and photic zone, while the top three microfacies (EMVII–EMIX) were deposited in a relatively deeper portion of the carbonate platform with normal salinity. SEM analysis indicated a dominant presence of first generation drusy cement throughout these lower-middle Eocene limestones and shales. This phenomenon indicates an early grade of post-depositional diagenesis (eogenetic) effects on these deposits. However, a minor amount of blocky (second generation) and rim (third generation) types of cement are also observed in the middle of the section, which indicates mesogenetic and telogenetic diagenesis alterations, respectively. It can be observed that these post-depositional diagenetic stages are directly proportional to the cement generations. Petrological observations reveal fracture, channel, growth framework, and moldic types of porosities, which provide favorable conditions for producing high permeability. Regional tectonic stresses also enhance the development of diagenetic features. Moreover, the diagenetic changes, pore types, and porosity values have considerably enhanced the reservoir characteristics of these carbonate rocks. On the basis of fossils such as *Acervulinidae* spp., Eocene sponge, *Milliolid*

spp. (*Idalina grelaudae*), *Rotalia* spp., and *Saccammina grzybowskii*, the relative chronological age of these carbonate deposits is suggested as Early–Middle Eocene.

**Author Contributions:** Conceptualization, A.B., M.S.M. and R.Y.; data collection, A.B., M.S.M. and R.Y.; methodology, A.B., M.S.M., R.Y. and H.T.J.; software, A.B., M.S.M., R.Y. and H.T.J., writing—original draft preparation, A.B., M.S.M. and R.Y.; supervision, A.B., M.S.M. and R.Y.; writing—review and editing, M.Z., G.K., H.T.J. and A.B. All authors have read and agreed to the published version of the manuscript.

**Funding:** This study was financially supported by the China-ASEAN Maritime Cooperation Fund Project (grant No. 12120100500017001) and the National Natural Science Foundation of China (grant No. 41972146).

**Institutional Review Board Statement:** Not applicable.

**Informed Consent Statement:** Not applicable.

**Data Availability Statement:** The data used in this work is available on request to the corresponding author(s).

**Conflicts of Interest:** The authors declare no conflict of interest (financial or non-financial).

## References

- Martín-Martín, M.; Guerrero, F.; Tosquella, J.; Tramontana, M. Middle Eocene carbonate platforms of the westernmost Tethys. *Sediment. Geol.* **2021**, *415*, 105861. [[CrossRef](#)]
- Pomar, L.; Baceta, J.I.; Hallock, P.; Mateu-Vicens, G.; Basso, D. Reef building and carbonate production modes in the west-central Tethys during the Cenozoic. *Mar. Pet. Geol.* **2017**, *83*, 261–304. [[CrossRef](#)]
- Rivero-Cuesta, L.; Westerhold, T.; Alegret, L. The Late Lutetian Thermal Maximum (middle Eocene): First record of deep-sea benthic foraminiferal response. *Palaeogeogr. Palaeoclimatol. Palaeoecol.* **2020**, *545*, 109637. [[CrossRef](#)]
- Janjuhah, H.T. Sedimentology and Origin of Microporosity in Miocene Carbonate Platforms, Central Luconia, offshore Sarawak, Malaysia. Doctoral Dissertation, Universiti Teknologi PETRONAS, Perak, Malaysia, 2018.
- Tawfik, M.; El-Sorogy, A.; Moussa, M. Metre-scale cyclicity in Middle Eocene platform carbonates in northern Egypt: Implications for facies development and sequence stratigraphy. *J. Afr. Earth Sci.* **2016**, *119*, 238–255. [[CrossRef](#)]
- Fazal, A.G.; Umar, M.; Shah, F.; Miraj, M.A.F.; Janjuhah, H.T.; Kontakiotis, G.; Jan, A.K. Correction: Fazal et al. Geochemical Analysis of Cretaceous Shales from the Hazara Basin, Pakistan: Provenance Signatures and Paleo-Weathering Conditions. *J. Mar. Sci. Eng.* **2022**, *10*, 800. *J. Mar. Sci. Eng.* **2022**, *10*, 1654. [[CrossRef](#)]
- Mateen, A.; Wahid, A.; Janjuhah, H.T.; Mughal, M.S.; Ali, S.H.; Siddiqui, N.A.; Shafique, M.A.; Koumoutsakou, O.; Kontakiotis, G. Petrographic and Geochemical Analysis of Indus Sediments: Implications for Placer Gold Deposits, Peshawar Basin, NW Himalaya, Pakistan. *Minerals* **2022**, *12*, 1059. [[CrossRef](#)]
- Bilal, A.; Mughal, M.S.; Janjuhah, H.T.; Ali, J.; Niaz, A.; Kontakiotis, G.; Antonarakou, A.; Usman, M.; Hussain, S.A.; Yang, R. Petrography and Provenance of the Sub-Himalayan Kuldana Formation: Implications for Tectonic Setting and Palaeoclimatic Conditions. *Minerals* **2022**, *12*, 794. [[CrossRef](#)]
- Bilal, A.; Yang, R.; Fan, A.; Mughal, M.S.; Li, Y.; Basharat, M.; Farooq, M. Petrofacies and diagenesis of Thanetian Lockhart Limestone in the Upper Indus Basin (Pakistan): Implications for the Ceno-Tethys Ocean. *Carbonates Evaporites* **2022**, *37*, 78. [[CrossRef](#)]
- Hottinger, L.; Bassi, D. *Paleogene Larger Rotaliid Foraminifera from the Western and Central Neotethys*; Springer: Berlin/Heidelberg, Germany, 2014.
- Hallock, P. Symbiont-bearing foraminifera: Harbingers of global change? *Micropaleontology* **2000**, *46*, 95–104.
- El-Azabi, M. Sedimentological characteristics, palaeoenvironments and cyclostratigraphy of the middle Eocene sequences in Gabal el-Ramliya, Maadi-Sukhna stretch, north eastern Desert. In Proceedings of the Egyptian 8th International Conference on the Geology of Arab World, Cairo, Egypt, 13–16 February 2006; pp. 1–31.
- Swati, M.A.F.; Haneef, M.; Ahmad, S.; Naveed, Y.; Zeb, W.; Akhtar, N.; Owais, M. Biostratigraphy and depositional environments of the Early Eocene Margalla Hill Limestone, Kohala-Bala area, Haripur, Hazara Fold-Thrust Belt, Pakistan. *J. Himal. Earth Sci.* **2013**, *46*, 65.
- Shah, S.M.I. Stratigraphy of Pakistan (memoirs of the geological survey of Pakistan). *Geol. Surv. Pak.* **2009**, *22*, 1–8.
- Muhammad, S.; Khalid, P. Hydrogeophysical investigations for assessing the groundwater potential in part of the Peshawar basin, Pakistan. *Environ. Earth Sci.* **2017**, *76*, 494. [[CrossRef](#)]
- Iqbal, M.F.; Malik, A.H. Investigation of limestone exploitation area and its environmental impacts using GIS/RS techniques: A case study of Margalla Hills National Park, Islamabad. *J. Himal. Earth Sci.* **2010**, *43*, 31.

17. Mughal, M.S.; Zhang, C.; Du, D.; Zhang, L.; Mustafa, S.; Hameed, F.; Khan, M.R.; Zaheer, M.; Blaise, D. Petrography and provenance of the Early Miocene Murree Formation, Himalayan Foreland Basin, Muzaffarabad, Pakistan. *J. Southeast Asian Earth Sci.* **2018**, *162*, 25–40. [[CrossRef](#)]
18. Salih, H.D. Larger benthic foraminiferal assemblages from Sinjar Formation, SW Sulaimaniyah City Kurdistan Region, Iraq. *Iraqi Bull. Geol. Min.* **2012**, *8*, 1–17.
19. Mirza, K.; Akhter, N.; Ejaz, A.; Zaidi, S.F.A. Biostratigraphy, microfacies and sequence stratigraphic analysis of the Chorgali Formation, Central Salt Range, northern Pakistan. *Solid Earth Sci.* **2022**, *7*, 104–125. [[CrossRef](#)]
20. Ali, A. Sedimentology of the Chor Gali Formation, Central Salt Range Pakistan. Master's Thesis, Institute of Geology, University of the Punjab, Lahore, Pakistan, 2012. Volume 121, *Unpublished*.
21. Yasin, M.; Umar, M.; Rameez, S.; Samad, R. Biostratigraphy of early eocene margala hill limestone in the muzaffarabad area (Kashmir Basin, Azad Jammu and Kashmir). *Pak. J. Geol. (PJG)* **2017**, *1*, 16–20.
22. Dunham, R.J. *Classification of Carbonate Rocks According to Depositional Textures*; AAPG: Tulsa, OK, USA, 1962.
23. Rahimi, A.; Adabi, M.; Aghanabati, A.; Majidifard, M.; Jamali, A. Dolomitization mechanism based on petrography and geochemistry in the Shotori Formation (Middle Triassic), Central Iran. *Open J. Geol.* **2016**, *6*, 1149–1168. [[CrossRef](#)]
24. Gregg, J.M.; Sibley, D.F. Epigenetic Dolomitization and the Origin of Xenotopic Dolomite Texture: REPLY. *J. Sediment. Res.* **1986**, *56*, 735–736.
25. Janjuhah, H.T.; Ahmed Salim, A.M.; Ali, M.Y.; Ghosh, D.P.; Amir Hassan, M.H. Development of carbonate buildups and reservoir architecture of Miocene carbonate platforms, Central Luconia, offshore Sarawak, Malaysia. In Proceedings of the SPE/IATMI Asia Pacific Oil & Gas Conference and Exhibition, online, 12–14 October 2021.
26. Ahmad, I.; Shah, M.M.; Janjuhah, H.T.; Trave, A.; Antonarakou, A.; Kontakiotis, G. Multiphase Diagenetic Processes and Their Impact on Reservoir Character of the Late Triassic (Rhaetian) Kingriali Formation, Upper Indus Basin, Pakistan. *Minerals* **2022**, *12*, 1049. [[CrossRef](#)]
27. Sibley, D.F. *Climatic Control of Dolomitization, Seroe Domi Formation (Pliocene), Bonaire, NA*; AAPG: Tulsa, OK, USA, 1980.
28. Coppard, S.E.; Campbell, A.C. Taxonomic significance of test morphology in the echinoid genera *Diadema* Gray, 1825 and *Echinothrix* Peters, 1853 (Echinodermata). *ZOOSYSTEMA-PARIS-* **2006**, *28*, 93.
29. Janjuhah, H.T.; Alansari, A.; Santha, P.R. Interrelationship Between Facies Association, Diagenetic Alteration and Reservoir Properties Evolution in the Middle Miocene Carbonate Build Up, Central Luconia, Offshore Sarawak, Malaysia. *Arab. J. Sci. Eng.* **2018**, *44*, 341–356. [[CrossRef](#)]
30. Janjuhah, H.T.; Gamez Vintaned, J.A.; Salim, A.M.A.; Faye, I.; Shah, M.M.; Ghosh, D.P. Microfacies and depositional environments of miocene isolated carbonate platforms from Central Luconia, Offshore Sarawak, Malaysia. *Acta Geol. Sin.-Engl. Ed.* **2017**, *91*, 1778–1796. [[CrossRef](#)]
31. Kroh, A.; Nebelsick, J.H. Echinoderms and Oligo-Miocene carbonate systems: Potential applications in sedimentology and environmental reconstruction. *Carbonate Syst. Dur. Oligocene–Miocene Clim. Transit.* **2010**, *42*, 201–228.
32. Özcan, E.; Okay, A.; Bürkan, K.; Yücel, A.; Özcan, Z. Middle-Late Eocene marine record of the Biga Peninsula, NW Anatolia, Turkey. *Geol. Acta Int. Earth Sci. J.* **2018**, *16*, 163–187.
33. Feng, Q.; Gong, Y.-M.; Riding, R. Mid-Late Devonian calcified marine algae and cyanobacteria, South China. *J. Paleontol.* **2010**, *84*, 569–587. [[CrossRef](#)]
34. Flügel, E.; Munnecke, A. *Microfacies of Carbonate Rocks: Analysis, Interpretation and Application*; Springer: Berlin/Heidelberg, Germany, 2010; Volume 976.
35. Yaseen, A.; Rajpar, A.R.; Munir, M.; Roohi, G. Micropaleontology of Lockhart Limestone (Paleocene), Nilawahon Gorge, Central Salt Range, Pakistan. *J. Himal. Earth Sci.* **2011**, *44*, 9–16.
36. Sameeni, S.J.; Haneef, M.; Shabbir, F.; Ahsan, N.; Ahmad, N. Biostratigraphic studies of Lockhart Limestone, Changlagali area, Nathiagali-Murree road, Hazara, northern Pakistan. *Sci. Int.* **2013**, *25*, 543–550.
37. Ahmad, S.; Kroon, D.; Rigby, S.; Hanif, M.; Imraz, M.; Ahmad, T.; Jan, I.U.; Ali, A.; Zahid, M.; Ali, F. Integrated paleoenvironmental, bio-and sequence-stratigraphic analysis of the late Thanetian Lockhart Limestone in the Nammal Gorge section, western Salt Range, Pakistan. *J. Himal. Earth Sci.* **2014**, *47*, 16–23.
38. Janjuhah, H.T.; Sanjuan, J.; Alquadah, M.; Salah, M.K. Biostratigraphy, Depositional and Diagenetic Processes in Carbonate Rocks form Southern Lebanon: Impact on Porosity and Permeability. *Acta Geol. Sin.-Engl. Ed.* **2021**, *5*, 1668–1683. [[CrossRef](#)]
39. Mattes, B.W.; Mountjoy, E.W. *Burial Dolomitization of the Upper Devonian Miette Buildup, Jasper National Park, Alberta*; AAPG: Tulsa, OK, USA, 1980.
40. Janjuhah, H.T.; Salim, A.M.A.; Alansari, A.; Ghosh, D.P. Presence of microporosity in Miocene carbonate platform, Central Luconia, offshore Sarawak, Malaysia. *Arab. J. Geosci.* **2018**, *11*, 204. [[CrossRef](#)]
41. Basso, D.; Nalin, R.; Nelson, C.S. Shallow-water Sporolithon rhodoliths from north island (New Zealand). *Palaios* **2009**, *24*, 92–103. [[CrossRef](#)]
42. Sarkar, S. Microfacies analysis of larger benthic foraminifera-dominated Middle Eocene carbonates: A palaeoenvironmental case study from Meghalaya, NE India (Eastern Tethys). *Arab. J. Geosci.* **2017**, *10*, 121. [[CrossRef](#)]
43. Varrone, D.; d'Atri, A. Acervulinid macroid and rhodolith facies in the Eocene Nummulitic limestone of the Dauphinois Domain (Maritime Alps, Liguria, Italy). *Swiss J. Geosci.* **2007**, *100*, 503–515. [[CrossRef](#)]

44. Janjuhah, H.T.; Alansari, A.; Vintaned, J.A.G. Quantification of microporosity and its effect on permeability and acoustic velocity in Miocene carbonates, Central Luconia, offshore Sarawak, Malaysia. *J. Pet. Sci. Eng.* **2019**, *175*, 108–119. [[CrossRef](#)]
45. Astibia, H.; Elorza, J.; Pisera, A.; Alvarez-Pérez, G.; Payros, A.; Ortiz, S. Sponges and corals from the Middle Eocene (Bartonian) marly formations of the Pamplona Basin (Navarre, Western Pyrenees): Taphonomy, taxonomy, and paleoenvironments. *Facies* **2014**, *60*, 91–110. [[CrossRef](#)]
46. Leszczyński, S.; Kołodziej, B.; Bassi, D.; Malata, E.; Gasiński, M.A. Origin and re-sedimentation of rhodoliths in the Late Paleocene flysch of the Polish Outer Carpathians. *Facies* **2012**, *58*, 367–387. [[CrossRef](#)]
47. Janjuhah, H.T.; Alansari, A. Offshore carbonate facies characterization and reservoir quality of Miocene rocks in the southern margin of South China Sea. *Acta Geol. Sin.-Engl. Ed.* **2020**, *94*, 1547–1561. [[CrossRef](#)]
48. Murray, J.W.; Alve, E.; Jones, B.W. Palaeoclimatology, Palaeoecology. A new look at modern agglutinated benthic foraminiferal morphogroups: Their value in palaeoecological interpretation. *Palaeogeogr. Palaeoclim. Palaeoecol.* **2011**, *309*, 229–241. [[CrossRef](#)]
49. Stalder, C.; Vertino, A.; Rosso, A.; Rüggeberg, A.; Pirkenseer, C.; Spangenberg, J.E.; Spezzaferri, S.; Camozzi, O.; Rappo, S.; Hajdas, I. Microfossils, a key to unravel cold-water carbonate mound evolution through time: Evidence from the eastern Alboran Sea. *PLoS ONE* **2015**, *10*, e0140223. [[CrossRef](#)]
50. Reiss, Z.; Hottinger, L. *The Gulf of Aqaba: Ecological Micropaleontology*; Springer Science & Business Media: Berlin/Heidelberg, Germany, 2012; Volume 50.
51. Renema, W. Larger foraminifera as marine environmental indicators. *Scr. Geol.* **2002**, *124*, 1–260.
52. Baumgartner-Mora, C.; Baumgartner, P.O. Latest Miocene-Pliocene Larger Foraminifera and depositional environments of the carbonate bank of La Désirade Island, Guadeloupe (French Antilles). *Rev. Micropaléontologie* **2011**, *54*, 183–205. [[CrossRef](#)]
53. Banerjee, S.; Khanolkar, S.; Saraswati, P.K. Facies and depositional settings of the Middle Eocene-Oligocene carbonates in Kutch. *Geodin. Acta* **2018**, *30*, 119–136. [[CrossRef](#)]
54. Lin, Q.; Wang, J.; Algeo, T.J.; Su, P.; Hu, G. Formation mechanism of authigenic gypsum in marine methane hydrate settings: Evidence from the northern South China Sea. *Deep Sea Res. Part I Oceanogr. Res. Pap.* **2016**, *115*, 210–220. [[CrossRef](#)]
55. Koo, H.J.; Jang, J.K.; Lee, D.H.; Cho, H.G. Authigenic Gypsum Precipitation in the ARAON Mounds, East Siberian Sea. *Minerals* **2022**, *12*, 983. [[CrossRef](#)]
56. Kocherla, M. Authigenic Gypsum in Gas-Hydrate Associated Sediments from the East Coast of India (Bay of Bengal). *Acta Geol. Sin.-Engl. Ed.* **2013**, *87*, 749–760. [[CrossRef](#)]
57. Selley, R.C.; Cocks, L.R.M.; Plimer, I.R. *Encyclopedia of Geology*; Elsevier Academic: Amsterdam, The Netherlands, 2005.
58. Pierre, C.; Bayon, G.; Blanc-Valleron, M.-M.; Mascle, J.; Dupré, S. Authigenic carbonates related to active seepage of methane-rich hot brines at the Cheops mud volcano, Menes caldera (Nile deep-sea fan, eastern Mediterranean Sea). *Geo-Marine Lett.* **2014**, *34*, 253–267. [[CrossRef](#)]
59. Novikova, S.A.; Shnyukov, Y.F.; Sokol, E.V.; Kozmenko, O.A.; Semenova, D.V.; Kutny, V.A. A methane-derived carbonate build-up at a cold seep on the Crimean slope, north-western Black Sea. *Mar. Geol.* **2015**, *363*, 160–173. [[CrossRef](#)]
60. Beavington-Penney, S.J.; Wright, V.P.; Racey, A. The middle Eocene Seeb Formation of Oman: An investigation of acyclicity, stratigraphic completeness, and accumulation rates in shallow marine carbonate settings. *J. Sediment. Res.* **2006**, *76*, 1137–1161. [[CrossRef](#)]
61. Mehdi, H.; Vahidinia, M.; Hrabovsky, J. Larger foraminiferal biostratigraphy and microfacies analysis from the Ypresian (Ilerdian-Cuisian) limestones in the Sistan Suture Zone (eastern Iran). *Turk. J. Earth Sci.* **2019**, *28*, 122–145.
62. Anketell, J.; Mriheel, I. Depositional environment and diagenesis of the Eocene Jdeir Formation, Gabes-Tripoli basin, Western Offshore, Libya. *J. Pet. Geol.* **2000**, *23*, 425–447. [[CrossRef](#)]
63. Drobne, K.; Cosovic, V.; Moro, A.; Buckovic, D. The role of the Palaeogene Adriatic Carbonate Platform in the spatial distribution of Alveolinids. *Turk. J. Earth Sci.* **2011**, *20*, 721–751. [[CrossRef](#)]
64. Langer, M.R.; Hottinger, L. Biogeography of selected “larger” foraminifera. *Micropaleontology* **2000**, *46*, 105–126.
65. Zamagni, J.; Mutti, M.; Košir, A. Evolution of shallow benthic communities during the Late Paleocene–earliest Eocene transition in the Northern Tethys (SW Slovenia). *Facies* **2008**, *54*, 25–43. [[CrossRef](#)]
66. Yordanova, E.K.; Hohenegger, J. Taphonomy of larger foraminifera: Relationships between living individuals and empty tests on flat reef slopes (Sesoko Island, Japan). *Facies* **2002**, *46*, 169–203. [[CrossRef](#)]
67. Tomás, S.; Frijia, G.; Bömelburg, E.; Zamagni, J.; Perrin, C.; Mutti, M. Evidence for seagrass meadows and their response to paleoenvironmental changes in the early Eocene (Jafnayn Formation, Wadi Bani Khalid, N Oman). *Sediment. Geol.* **2016**, *341*, 189–202. [[CrossRef](#)]
68. Tomassetti, L.; Benedetti, A.; Brandano, M. Middle Eocene seagrass facies from Apennine carbonate platforms (Italy). *Sediment. Geol.* **2016**, *335*, 136–149. [[CrossRef](#)]
69. Beavington-Penney, S.J. Analysis of the effects of abrasion on the test of *Palaeonummulites venosus*: Implications for the origin of nummulithoclastic sediments. *Palaios* **2004**, *19*, 143–155. [[CrossRef](#)]
70. Prothero, D.R.; Schwab, F. *Sedimentary Geology*; Macmillan: New York, NY, USA, 2004.
71. Zielinski, J.P.T.; Vidal, A.C.; Chinelatto, G.F.; Coser, L.; Fernandes, C.P. Evaluation of pore system properties of coquinas from Morro do Chaves Formation by means of X-ray microtomography. *Braz. J. Geophys.* **2018**, *36*, 541–557. [[CrossRef](#)]

72. Amel, H.; Jafarian, A.; Husinec, A.; Koeshidayatullah, A.; Swennen, R.J.M.; Geology, P. Microfacies, depositional environment and diagenetic evolution controls on the reservoir quality of the Permian Upper Dalan Formation, Kish Gas Field, Zagros Basin. *Mar. Pet. Geol.* **2015**, *67*, 57–71. [[CrossRef](#)]
73. Janjuhah, H.T.; Kontakiotis, G.; Wahid, A.; Khan, D.M.; Zarkogiannis, S.D.; Antonarakou, A. Integrated Porosity Classification and Quantification Scheme for Enhanced Carbonate Reservoir Quality: Implications from the Miocene Malaysian Carbonates. *J. Mar. Sci. Eng.* **2021**, *9*, 1410. [[CrossRef](#)]
74. Abu-Hashish, M.F.; Afify, H.M. Effect of petrography and diagenesis on the sandstone reservoir quality: A case study of the Middle Miocene Kareem Formation in the North Geisum oil field, Gulf of Suez, Egypt. *Arab. J. Geosci.* **2022**, *15*, 465. [[CrossRef](#)]
75. Ali, S.K.; Janjuhah, H.T.; Shahzad, S.M.; Kontakiotis, G.; Saleem, M.H.; Khan, U.; Zarkogiannis, S.D.; Makri, P.; Antonarakou, A. Depositional Sedimentary Facies, Stratigraphic Control, Paleoecological Constraints, and Paleogeographic Reconstruction of Late Permian Chhidru Formation (Western Salt Range, Pakistan). *J. Mar. Sci. Eng.* **2021**, *9*, 1372. [[CrossRef](#)]